Natural Resources Canada | Ressources naturelles Canada

Preliminary in situ SHRIMP geochronological constraints on the tectonometamorphic evolution of Cumberland Peninsula, Baffin Island, Nunavut

R.G. Berman, M. Sanborn-Barrie, B.M. Hamilton, N. Rayner, and M. Young

Geological Survey of Canada
Current Research 2013-7

2013

Canada

Geological Survey of Canada
Current Research 2013-7

Preliminary in situ SHRIMP geochronological constraints on the tectonometamorphic evolution of Cumberland Peninsula, Baffin Island, Nunavut

R.G. Berman, M. Sanborn-Barrie, B.M. Hamilton, N. Rayner, and M. Young

2013

ISSN 1701-4387
Catalogue No. M44-2013/7E-PDF
ISBN 978-1-100-21689-8
doi: 10.4095/292215

A copy of this publication is also available for reference in depository libraries across Canada through access to the Depository Services Program's Web site at http://dsp-psd.pwgsc.gc.ca

This publication is available for free download through GEOSCAN http://geoscan.ess.nrcan.gc.ca

Recommended citation

Berman, R.G., Sanborn-Barrie, M., Hamilton, B.M., Rayner, N., and Young, M., 2013. Preliminary in situ SHRIMP geochronological constraints on the tectonometamorphic evolution of Cumberland Peninsula, Baffin Island, Nunavut; Geological Survey of Canada, Current Research 2013-7, 19 p. doi: 10.4095/292215

Critical review

D. Kellett

Authors

R.G. Berman
(Rob.Berman@NRCan-RNCan.gc.ca)
M. Sanborn-Barrie
(Mary.Sanborn-Barrie@NRCan-RNCan.gc.ca)
N. Rayner
(Nicole.Rayner@NRCan-RNCan.gc.ca)
Geological Survey of Canada
601 Booth Street
Ottawa, Ontario
K1A 0E8

B.M. Hamilton (brett.hamilton@ucalgary.ca)
Department of Geoscience
University of Calgary
Calgary, Alberta
T2N 1N4

M. Young (mdyoung@dal.ca)
Department of Earth Sciences
Dalhousie University
Halifax, Nova Scotia
B3H 4R2

Correction date:

Preliminary in situ SHRIMP geochronological constraints on the tectonometamorphic evolution of Cumberland Peninsula, Baffin Island, Nunavut

R.G. Berman, M. Sanborn-Barrie, B.M. Hamilton,
N. Rayner, and M. Young

Berman, R.G., Sanborn-Barrie, M., Hamilton, B.M., Rayner, N., and Young, M., 2013. Preliminary in situ SHRIMP geochronological constraints on the tectonometamorphic evolution of Cumberland Peninsula, Baffin Island, Nunavut; Geological Survey of Canada, Current Research 2013-7, 19 p. doi:10.4095/292215

Abstract: Preliminary in situ SHRIMP monazite geochronology on metasedimentary rocks from Cumberland Peninsula reveals a polycyclic metamorphic history that helps to provide a framework on which regional tectonic and metallogenic models for northeastern Laurentia can be built. One sample records Neoarchean monazite growth at 2785 ± 4 and 2701 ± 6 Ma, with the former interpreted to date an Archean deformation event (D_{A1}) recorded by the inclusion fabric within garnet. Three samples with monazite ages between 1897 ± 8 and 1881 ± 8 Ma are interpreted to record regional Paleoproterozoic contact metamorphism (M_{P1}) up to granulite facies related to emplacement of the Qikiqtarjuaq plutonic suite, with textural features consistent with D_{P1} deformation during pluton emplacement. Six samples distributed across Cumberland Peninsula record monazite crystallization between 1863 ± 5 and 1859 ± 7 Ma, interpreted to date the main amphibolite-facies tectonometamorphic event (M_{P2}-D_{P2}) event. The timing of this event is similar to that determined elsewhere in the Rae Craton (e.g. Southampton Island, western Committee Bay belt), and is considered to reflect the collision between Meta Incognita microcontinent and the Rae Craton. Monazite growth and/or recrystallization at ca. 1840 Ma (M_{P3}) in five samples and at 1805 ± 6 Ma (M_{P4}) in one sample is interpreted to have occurred after the thermal peak, during late- to post-tectonic, amphibolite-facies metamorphism.

Résumé : Une étude géochronologique préliminaire des roches métasédimentaires de la péninsule Cumberland, réalisée par datation *in situ* de la monazite à la microsonde SHRIMP, révèle une histoire métamorphique polycyclique qui contribue à fournir un cadre sur lequel peuvent s'appuyer les modèles tectoniques et métallogéniques régionaux pour le nord-est de la Laurentie. L'un des échantillons rend compte de la croissance de la monazite au Néoarchéen à 2785 ± 4 et à 2701 ± 6 Ma, cette dernière période permettrait, selon notre interprétation, de dater un épisode de déformation à l'Archéen (D_{A1}) indiqué par la fabrique des inclusions dans le grenat. Trois échantillons, pour lesquels les âges de la monazite se situent entre 1897 ± 8 et 1881 ± 8 Ma, permettent d'interpréter un métamorphisme de contact régional au Paléoprotérozoïque (M_{P1}) jusqu'au faciès des granulites associé à la mise en place de la suite plutonique de Qikiqtarjuaq, avec des caractéristiques texturales qui concordent avec la déformation D_{P1} pendant la mise en place des plutons. Six échantillons répartis dans toute la péninsule Cumberland indiquent une cristallisation de la monazite entre 1863 ± 5 et 1859 ± 7 Ma, permettant de dater le principal événement tectonométamorphique au faciès des amphibolites (M_{P2}-D_{P2}). Le moment où est survenu cet événement est similaire à celui qui a été déterminé ailleurs dans le craton de Rae (p. ex. île Southampton, ouest de la ceinture de Committee Bay), et reflèterait la collision entre le microcontinent Meta Incognita et le craton de Rae. La croissance ou la recristallisation de la monazite, vers 1840 Ma (M_{P3}) d'après cinq échantillons et à 1805 ± 6 Ma (M_{P4}) d'après un autre échantillon, aurait eu lieu après le pic thermique, pendant le métamorphisme tarditectonique à post-tectonique au faciès des amphibolites.

INTRODUCTION

The Geo-mapping for Energy and Minerals (GEM) Cumberland Peninsula (CP) project was initiated to provide integrated geoscience knowledge for an underexplored 58 000 km^2 area of eastern Baffin Island. This region had only been examined at a (1:1 million) reconnaissance scale and, as such, presented a major knowledge gap in the context of resource-based economic development and sustainability of Canada's north. Metamorphic studies undertaken as part of this integrated geoscience project provide insight into the region's magmatic and tectonic evolution, from which regional metallogenic models supporting exploration for diamonds, precious-, and base-metals are better constrained. This paper reports the results of in situ Sensitive High Resolution Ion Microprobe (SHRIMP) monazite geochronology from eight metasedimentary samples collected across the peninsula, augmented by preliminary thermobarometric estimates for some of the dated samples. While these data provide initial insights to the tectonothermal evolution of this region, detailed research into all aspects of the metamorphic character and history of Cumberland Peninsula is ongoing by Ph.D. candidate B. Hamilton at University of Calgary.

REGIONAL GEOLOGICAL SETTING

Cumberland Peninsula is situated on eastern Baffin Island (Fig. 1) in a region that has been postulated to represent either the eastern extension of the Archean Rae Craton (St-Onge et al., 2009) or the northwestern extension of the North Atlantic Craton (e.g. Corrigan et al., 2009). Recent mapping (Sanborn-Barrie et al., 2011a, b, c; Sanborn-Barrie and Young, 2013a, b, c; Sanborn-Barrie et al., 2013a, b and geochronology (Rayner et al., 2012) reveal that Archean (2.97–2.76 Ga) tonalite-granodiorite-trondhjemite basement underlies about 60% of Cumberland Peninsula (Fig. 2). Strands of Archean semipelite±psammite, amphibolite, rare pillowed volcanic rocks and ca. 2.91 Ga porphyry form a minor, yet significant component of Cumberland Peninsula's basement complex.

In contrast to previous geological compilations of Baffin Island, recent mapping has established that a Paleoproterozoic cover sequence, designated the Hoare Bay group (Jackson, 1971), forms a northeast-trending belt across central Cumberland Peninsula (Fig. 2). The group comprises thick successions of psammite-semipelite, suggesting a basinal facies in the east, and includes minor marble, calc-silicate, and orthoquartzite which may represent remnants of a shelf succession in the west part of the peninsula. The contact between the Paleoproterozoic Hoare Bay group and Archean basement rocks is poorly exposed, but, where evident, is

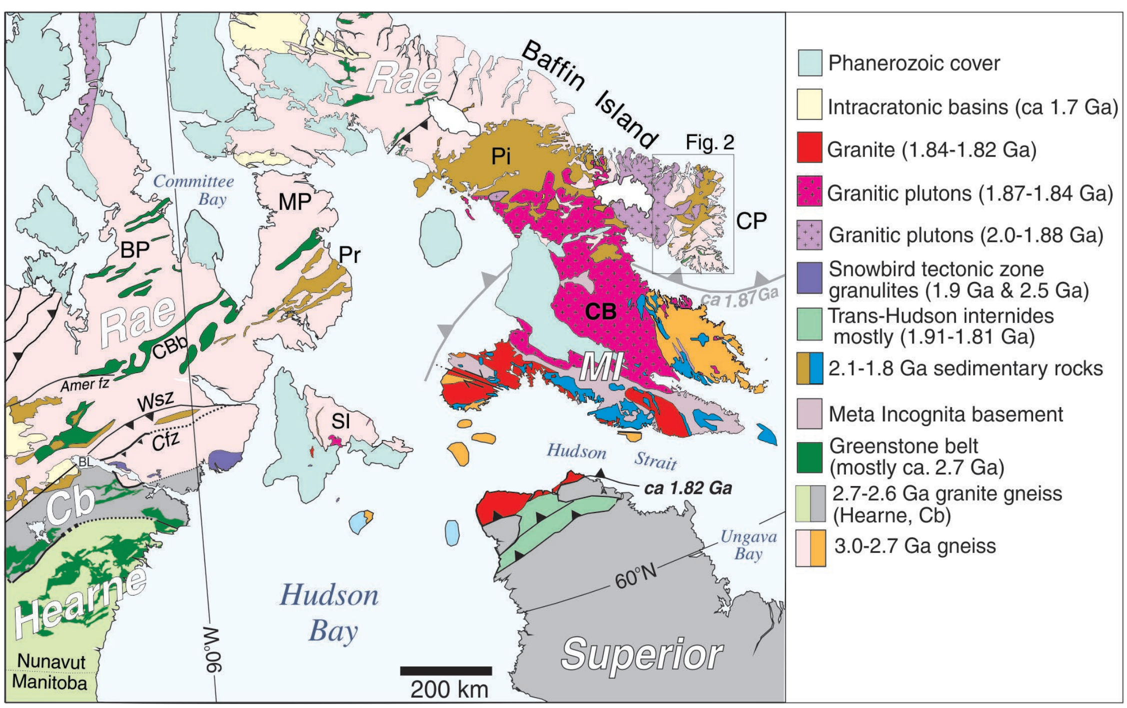

Figure 1. Regional geology of the Precambrian core of Laurentia flanking Hudson Bay, modified from Berman et al. (2005). Abbreviations: BL = Baker Lake, CBb = Committee Bay belt, Cb = Chesterfield block; CB = Cumberland Batholith, Cfz = Chesterfield fault zone, MI = Meta Incognita microcontinent, MP = Melville Peninsula, Pr = Penrhyn group, Pi = Piling Group; SI = Southampton Island, Wsz = Wager Bay shear zone.

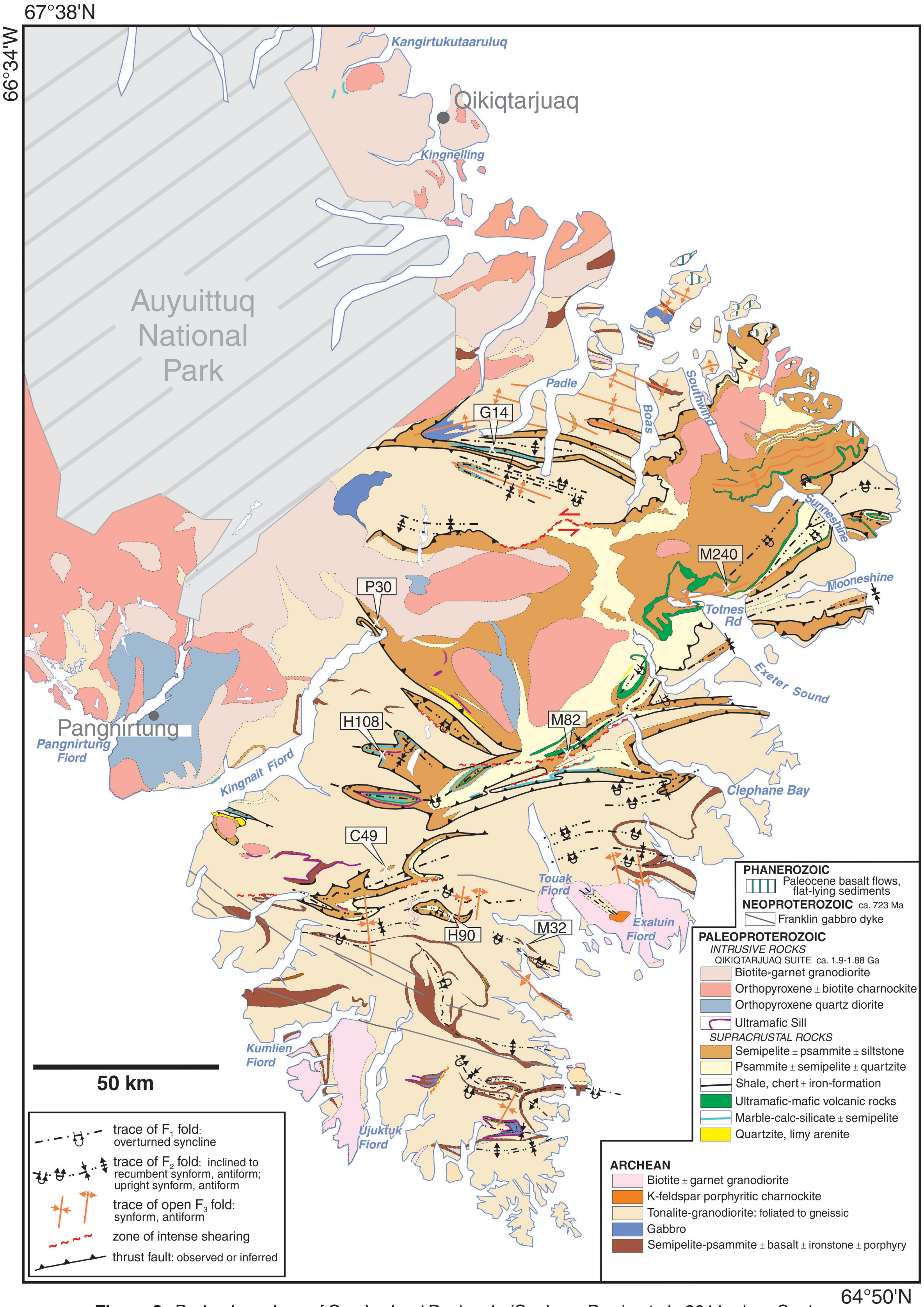

Figure 2. Bedrock geology of Cumberland Peninsula (Sanborn-Barrie et al., 2011a, b, c; Sanborn-Barrie and Young, 2013a, b, c; Sanborn-Barrie et al., 2013a, b) showing location of the eight semipelite samples targeted for this geochronological study.

strongly deformed, and hence is known or inferred to be tectonic. A belt of ca. 1.9 Ga granodiorite-charnockite-quartz diorite (Qikiqtarjuaq plutonic suite) that cuts, and thermally overprints, cover strata and some basement, extends over 200 km from Pangnirtung to Qikiqtarjuaq (Fig. 2).

At least two penetrative deformation events have affected much of Cumberland Peninsula resulting in pervasive tight to isoclinal, inclined to recumbent F_2 folds of both basement and cover rocks. Where preserved or only weakly transposed, S_1 is generally bedding-parallel and northwest-dipping. Shallowly to moderately north-dipping S_1+S_2 transposition fabrics and F_2 folds reflect widespread south-vergent D_2 structures. A younger compressional event locally modifies the peninsula's strong, flat-lying S_1+ S_2 transposition fabric into upright F_3 folds or broad open warps.

Hamilton et al. (2012) present a metamorphic map for the region based on preliminary compilation of field observations and petrographic assessments. Metamorphic grade ranges from lower-amphibolite facies (staurolite± andalusite±sillimanite in muscovite-bearing metapelites) to lower-granulite facies (cordierite+garnet+K-feldspar in migmatitic metapelite; orthopyroxene in metabasite and metasemipelite), with the majority of the region being of upper-amphibolite facies (garnet+sillimanite±K-feldspar in variably migmatitic metapelites). Granulite-facies regions typically show some evidence of an amphibolite-facies overprint. Petrographic relationships suggest that, at least for one metamorphic event, the prograde crystallization sequence was staurolite-andalusite-sillimanite in some metapelitic samples, which constrains pressures for the lower-amphibolite facies domain to 3.3 to 4.1 kbar (Hamilton et al., 2012).

METHODS

Eight, widely distributed metasedimentary samples were chosen to attain an overview of the timing of tectonometamorphism of this region (Fig. 2). In order to gain insight into its early history prior to, and potentially related to, assembly of Laurentia, the primary targets were monazite inclusions in porphyroblasts that may have been shielded from re-equilibration during later metamorphism. All samples contained monazite of a size (>10 μm) suitable for in situ SHRIMP analysis, carried out on 3 mm diameter cores drilled from texturally significant areas of polished thin sections according to the methods of Rayner and Stern (2002). A small plug of pre-polished laboratory standard monazites (GSC monazite z8152, z3345, and z2908) was included on the mount. Further details of the analytical methodology are described in Stern and Berman (2001). Analyses were conducted during two analytical sessions on two separate mounts. Details regarding the spot size, data-reduction protocol, and U-Pb calibration are reported in the footnotes of the data table. Common Pb correction utilized the Pb composition of the surface blank (Stern, 1997). A Pb fractionation correction of +0.9% was applied to some of the Pb-isotope data, the magnitude of which was determined by the analysis of monazite standards z3345 and z2908 whose $^{207}Pb/^{206}Pb$ ages have been determined by isotope-dilution methods (Stern and Berman, 2001). The error associated with the mass fractionation correction has been added quadratically to the isotopic ratio error when calculating weighted mean ages.

Preliminary P –T conditions of some of the dated samples were calculated using the winTWQ software (version 2.35; Berman, 2007). Thermobarometric errors are estimated at ± 1 kbar, 50°C (Berman, 1991). To further support these results, mineral assemblages and compositions were computed from whole-rock compositions with DOMINO software (de Capitani and Petrakakis, 2010), following the methodology summarized by Berman et al. (2005). Unless otherwise noted, limited compositional variations were observed in matrix plagioclase (<0.02 X_{An}) and biotite (<0.02 in Fe/(Fe+Mg)), except where the latter contacts garnet. Reported P-T data were derived from the rim compositions of nearby garnet and biotite that are separated by quartz and/or plagioclase.

GEOCHRONOLOGICAL CONSTRAINTS LINKED TO METAMORPHIC EVOLUTION

Table 1 summarizes geochronological results for the eight samples (Fig. 2). Table 2 provides SHRIMP analytical data for monazite. Concordia diagram ellipses and errors of mean ages are reported in the text at 2σ. Below, we present the geological context, textural relationships, preliminary thermobarometric results, and geochronological results for these eight samples.

09SRB-M32 (GSC lab number 10215)

Semipelite with an assemblage of garnet-biotite-sillimanite-K-feldspar-plagioclase-quartz was collected from southern Cumberland Peninsula from a rare 2 m wide supracrustal panel (Fig. 3a) that occurs within tonalite in a region where the tonalitic±gabbroic basement complex is consistently overturned into gently inclined, south-vergent F_2 folds. The sample exhibits the regional transposition foliation (S_1+S_2) oriented 305/36 with a shallow L_2 lineation plunging 12° to the northwest (336°). The foliation is defined dominantly by biotite and minor sillimanite, with concordant leucocratic bands interpreted to represent crystallized melt. Garnet porphyroblasts range from 2 mm to 1 cm in diameter. Smaller porphyroblasts generally cut the foliation, whereas the largest porphyroblast is wrapped by the foliation. Accordingly, small garnet porphyroblasts appear post-tectonic, whereas large porphyroblasts appear pre- to syn-tectonic.

Table 1. Summary of SHRIMP U-Pb in situ monazite ages.

Sample #	Porphyroblasts	Age ± 2σ	Monazite textures
M_{A1}-D_{A1} @ 2.79 and M_{A2} @ 2.70 Ga			
09SRB-M32	Grt	2785 ± 4	equant-elongate inclusions within S_{int} in Grt
		2701 ± 6	Grt inclusion not associated with S_{int}
M_{P1}-D_{P1} @ 1.89–1.88 Ga			
09SRB-P30	Grt-Sil	1897 ± 8	Grt inclusion with randomly oriented Sil
09SRB-H108	Grt-Sil	1881 ± 8	Grt inclusion within S_{int}
10SRB-M240	Grt-And-St	1890 ± 7	And-Grt inclusions within weak S_{int}
M_{P2}-D_{P2} @ 1.86 Ga			
09SRB-P30	Grt-Sil	1862 ± 12	elongate matrix grains || S_2 foln
09SRB-H108	Grt-Sil	1864 ± 27	elongate matrix grain || S_2 foln
09SRB-H90	Grt-Sil	1860 ± 5	equant inclusions within weak S_{int} in Grt
09SRB-C49	Grt-Sil	1859 ± 7	elongate matrix grains || S_2 foln
09SRB-M82	Grt-St-Sil	1863 ± 5	elongate matrix grains mostly || S_2 foln
10SRB-G14	Grt-Sil	1861 ± 4	elongate matrix grains || S_2 foln
M_{P3} @ 1.84 Ga			
09SRB-M32	Grt	1841 ± 12	moderate-Y rim of matrix grain
09SRB-M82c	Grt-St-Sil	1841 ± 9	post-D2 matrix grain
10SRB-G14	Grt-Sil	1840 ± 3	matrix grain rims; Grt inclusions w fractures
M_{P4} @ 1.81 Ga			
10SRB-M240	Grt-And-St	1805 ± 6	matrix grain rims; Grt inclusions w fractures
S_{int} = planar fabric within porphyroblast			

A 1 cm wide garnet porphyroblast has a calcic rim (X_{Grs} = 0.05–0.06; Fe/(Fe+Mg) = 0.66–0.67) extending inward ~350 µm to a textural break in the orientation of quartz inclusions (Fig. 3b) before decreasing over ~1200 µm to the typical core composition (X_{Grs} = 0.018–0.020, Fe/(Fe+Mg) = 0.66–0.67). MnO decreases very slightly from core to rim (X_{Sps} = 0.032–0.029). The coincidence of the textural break with more calcic rims suggest garnet rim growth during a significantly higher pressure event than garnet core growth. Preliminary thermobarometric estimates for rim growth are 8 kbar and 750°C, in good agreement with phase-diagram calculations.

Ten SHRIMP analyses of three monazite inclusions (#17, 20, 31) in the core of the large garnet porphyroblast (Fig. 3b) and the equant, high-Y core of matrix grain #181 (Fig. 3c, inset) collectively yielded a weighted mean $^{207}Pb/^{206}Pb$ age of 2785 ± 4 Ma (Mean Square of Weighted Deviates - MSWD = 0.20). Although inclusion grains #17 and #20 are equant, grain #31 (Fig. 3c, inset) is moderately elongate parallel to the quartz inclusion fabric in this garnet (Fig. 3b). Three analyses of two spots on grain #52, an inclusion in a garnet porphyroblast with no internal fabric, yield a weighted mean $^{207}Pb/^{206}Pb$ age of 2701 ± 6 Ma (MSWD = 0.29; Fig. 3c). Two replicate analyses of the moderate-Y rim of monazite #181 (Fig. 3c, inset), a moderately elongate, foliation-parallel matrix grain, yield an average age of 1841 ± 12 (MSWD = 1.06). The third analysis of this same spot (#181.2.3) gives a younger ca. 1790 Ma age, apparently sampling a younger age domain on the rim of this grain. A ca. 1980 Ma spot age obtained from the opposite tip of this grain (analysis #181.3) appears to represent a mixed age.

09SRB-P30 (GSC lab number 10217)

Metapelitic rocks near the head of Kingnait Fiord (Fig. 2) generally contain the assemblage garnet-biotite-sillimanite-plagioclase-quartz±cordierite (Hamilton et al., 2012). A sample of semipelite lacking cordierite contains coarse sillimanite and biotite that define a strong foliation (137/55), which parallels both an observed basement-cover thrust fault located 1.5 km to the southwest and an intrusive contact of a 1894 ± 6 Ma Qikiqtarjuaq suite pluton (Rayner et al., 2012) located 2 km to the northeast (Fig. 2). This main foliation is crenulated (Fig. 4a) at the sampling site with microfold axes plunging 47° west (263°), parallel to the local down-dip lineation.

Most garnet porphyroblasts are elongate parallel to the main foliation with aspect ratios typically higher than 4:1, but more equant garnet porphyroblasts also occur. A coherent

Table 2. SHRIMP U-Pb monazite results.

Spot	Location	U (ppm)	Th (ppm)	Th/U	$^{206}Pb^*$ (ppm)	$^{204}Pb/^{206}Pb$	% ±	$f(206)^{204}$ (%)	$^{208*}Pb/^{206*}Pb$	% ±	$^{207*}Pb/^{235}U$	% ±	$^{206*}Pb/^{238}U$	% ±	Corr Coeff	$^{207*}Pb/^{206*}Pb$	% ±	Apparent Ages (Ma) $^{206}Pb/^{238}U$	± $^{206}Pb/^{238}U$	$^{207}Pb/^{206}Pb$	± $^{207}Pb/^{206}Pb$	Disc. (%)
09SRB-M32 - z10215 (UTM zone 20; 472755E 7276441N) - IP556																						
17.1.1	Grt,eq	2275	28463	12.9	1052	2.5E-5	33	0.043	3.8	0.24	14.47	1.1	0.538	1.09	0.988	0.195	0.171	2776	25	2784	3	0.3
17.1.2	Grt,eq	2945	34061	11.9	1318	2.5E-5	29	0.043	3.4	0.41	14.02	1.1	0.521	1.13	0.984	0.195	0.201	2703	25	2787	3	3.0
17.1.3	Grt,eq	3235	36372	11.6	1466	2.3E-5	34	0.040	3.2	0.33	14.17	1.2	0.527	1.14	0.981	0.195	0.223	2730	25	2784	4	1.9
17.1.4	Grt,eq	4542	55158	12.5	2125	1.2E-5	99	0.020	3.7	0.48	14.67	1.2	0.545	1.19	0.979	0.195	0.248	2803	27	2787	4	-0.6
20.1	Grt,eq	2263	24915	11.4	1004	2.7E-4	7	0.472	3.3	0.38	13.81	1.1	0.517	1.11	0.981	0.194	0.220	2685	24	2776	4	3.3
20.2	Grt,eq	2086	26446	13.1	912	3.6E-4	7	0.626	3.7	0.32	13.66	1.2	0.509	1.14	0.971	0.195	0.278	2652	25	2782	5	4.7
31.1	Grt,S1	2386	26999	11.7	1090	2.8E-5	32	0.049	3.4	0.36	14.29	1.1	0.532	1.10	0.987	0.195	0.179	2749	25	2784	3	1.3
31.1.2	Grt,S1	2583	28272	11.3	1140	1.4E-5	58	0.024	3.3	0.37	13.85	1.1	0.514	1.11	0.986	0.195	0.186	2673	24	2788	3	4.1
31.2	Grt,S1	2361	25228	11.0	1050	3.4E-5	41	0.059	3.3	0.29	13.94	1.1	0.518	1.10	0.982	0.195	0.210	2689	24	2787	3	3.5
181.1	mat,eq	2516	8249	3.4	1107	1.1E-5	44	0.020	0.9	0.38	13.77	1.1	0.512	1.09	0.991	0.195	0.151	2666	24	2785	2	4.3
181.2	mat, S2	1441	17663	12.7	396	1.6E-4	17	0.277	3.7	0.42	4.98	1.3	0.320	1.17	0.921	0.113	0.495	1790	18	1847	9	3.1
181.2.2	mat, S2	1585	17544	11.4	410	1.4E-4	16	0.238	3.4	0.42	4.66	1.2	0.301	1.17	0.934	0.112	0.445	1697	17	1835	8	7.5
181.2.3	mat, S2	2086	21995	10.9	536	2.2E-4	13	0.376	3.3	0.44	4.52	1.3	0.299	1.18	0.916	0.110	0.515	1687	17	1794	9	5.9
181.3	mat, S2	1478	16375	11.4	393	1.7E-4	16	0.300	3.5	0.42	5.19	1.2	0.310	1.15	0.926	0.122	0.468	1740	18	1980	8	12.1
52.1	Grt,eq	1186	24301	21.2	516	5.5E-5	25	0.096	5.8	0.38	12.92	1.2	0.506	1.15	0.978	0.185	0.244	2640	25	2700	4	2.2
52.2	Grt,eq	1320	31577	24.7	566	2.9E-5	56	0.051	7.0	0.39	12.74	1.3	0.499	1.32	0.979	0.185	0.272	2611	28	2699	4	3.3
52.2.2	Grt,eq	1464	35981	25.4	620	8.3E-5	20	0.144	7.0	0.43	12.62	1.2	0.493	1.19	0.971	0.186	0.293	2584	25	2704	5	4.4
09SRB-P30 - z10217 (UTM zone 20; 438721E 7360954N) - IP556																						
14.1	Grt,eq	2599	35318	14.0	754	5.0E-5	38	0.087	3.9	0.31	5.39	1.2	0.338	1.11	0.956	0.116	0.342	1876	18	1893	6	0.9
14.2	Grt,eq	3609	29919	8.6	1032	1.5E-5	33	0.026	2.5	0.32	5.34	1.1	0.333	1.09	0.977	0.116	0.236	1853	18	1899	4	2.4
16.1	mat,S2	1120	11066	10.2	299	2.1E-4	16	0.369	3.0	0.50	4.84	1.3	0.311	1.21	0.901	0.113	0.583	1745	18	1846	11	5.5
16.1.2	mat,S2	1297	12763	10.2	334	2.0E-4	18	0.348	3.1	0.54	4.68	1.4	0.300	1.23	0.892	0.113	0.624	1691	18	1852	11	8.7
16.1.3	mat,S2	1455	14205	10.1	377	3.2E-4	15	0.558	3.2	0.60	4.66	1.7	0.302	1.46	0.882	0.112	0.777	1700	22	1830	14	7.1
16.1.4	mat,S2	1746	17177	10.2	485	2.3E-4	23	0.397	3.2	0.67	5.07	1.5	0.324	1.30	0.837	0.114	0.847	1807	20	1859	15	2.8
18.1	mat,S2	1541	4989	3.3	420	3.9E-5	35	0.068	1.0	0.67	5.02	1.2	0.317	1.16	0.954	0.115	0.364	1776	18	1876	7	5.3
18.2	mat,S2	1475	4427	3.1	398	9.3E-5	27	0.161	0.9	0.77	4.90	1.3	0.314	1.17	0.927	0.113	0.471	1760	18	1853	9	5.0
18.3	mat,S2	1870	8293	4.6	487	2.2E-5	43	0.038	1.3	0.63	4.76	1.2	0.303	1.16	0.952	0.114	0.373	1708	17	1860	7	8.1
18.4	mat,S2	1782	4758	2.8	449	2.1E-5	38	0.036	0.8	0.81	4.63	1.3	0.294	1.27	0.959	0.114	0.375	1659	19	1872	7	11.3
09SRB-H108 - z 10219 (UTM zone 20; 437700E 7327084N) - IP556																						
291.1	Grt,S1	1835	24289	13.7	525	1.3E-4	15	0.231	4.3	0.43	5.27	1.2	0.333	1.11	0.951	0.115	0.361	1853	18	1878	6	1.4
291.2	Grt,S1	2784	25428	9.4	754	1.0E-4	15	0.182	3.0	0.36	5.01	1.2	0.315	1.11	0.957	0.115	0.337	1767	17	1882	6	6.1
291.3	Grt,S1	4281	41687	10.1	1185	6.3E-5	20	0.109	2.9	0.33	5.12	1.5	0.322	1.43	0.980	0.115	0.291	1801	22	1883	5	4.4
527.1	mat,S2	4545	21577	4.9	1278	1.1E-5	59	0.019	1.5	0.34	5.17	1.1	0.327	1.11	0.983	0.115	0.204	1825	18	1873	4	2.6
527.2	mat,S2,r	6041	29443	5.0	1734	1.9E-5	41	0.033	1.4	0.36	5.15	1.1	0.334	1.07	0.979	0.112	0.224	1858	17	1828	4	-1.7
527.3	mat,S2	5790	27492	4.9	1596	10.0E-6	75	0.017	1.5	0.35	5.05	1.1	0.321	1.07	0.980	0.114	0.218	1794	17	1866	4	3.9
527.4	mat,S2,r	4936	22974	4.8	1350	3.0E-5	25	0.051	1.5	0.34	4.87	1.1	0.318	1.07	0.980	0.111	0.217	1782	17	1813	4	1.7
527.5	mat,S2	4323	22104	5.3	1176	3.1E-5	25	0.054	1.6	0.34	4.94	1.1	0.317	1.07	0.979	0.113	0.224	1773	17	1852	4	4.3

Table 2. (Cont.)

																		Apparent Ages (Ma)				
Spot	Location	U (ppm)	Th (ppm)	$\frac{Th}{U}$	$^{206}Pb^{*}$ (ppm)	$\frac{^{204}Pb}{^{206}Pb}$	% ±	$f(206)^{204}$ (%)	$\frac{^{208*}Pb}{^{206*}Pb}$	% ±	$\frac{^{207*}Pb}{^{235}U}$	% ±	$\frac{^{206*}Pb}{^{238}U}$	% ±	Corr Coeff	$\frac{^{207*}Pb}{^{206*}Pb}$	% ±	$\frac{^{206}Pb}{^{238}U}$	$\pm\frac{^{206}Pb}{^{238}U}$	$\frac{^{207}Pb}{^{206}Pb}$	$\pm\frac{^{207}Pb}{^{206}Pb}$	Disc. (%)
09SRB-H90 - z10218 (UTM zone 20; 452472E 7285624N) - IP556																						
1.1.1	Grt,eq	5751	34039	6.1	1596	1.6E-4	10	0.285	1.8	0.38	5.07	1.1	0.323	1.10	0.962	0.114	0.313	1805	17	1861	6	3.0
1.1.2	Grt,eq	5377	36532	7.0	1502	9.4E-5	13	0.163	2.1	0.36	5.09	1.1	0.325	1.10	0.967	0.114	0.289	1815	17	1858	5	2.3
1.1.3	Grt,eq	5720	43102	7.8	1604	1.2E-4	12	0.201	2.4	0.37	5.10	1.1	0.326	1.10	0.963	0.113	0.308	1821	18	1853	6	1.7
137.1	Grt,eq	5969	22281	3.9	1663	2.5E-5	22	0.044	1.2	0.30	5.09	1.1	0.324	1.13	0.989	0.114	0.168	1811	18	1861	3	2.7
137.1.2	Grt,eq	7010	27778	4.1	1898	8.1E-6	57	0.014	1.2	0.32	4.94	1.1	0.315	1.06	0.986	0.114	0.178	1766	16	1858	3	5.0
137.1.3	Grt,eq	8606	32962	4.0	2377	1.1E-5	38	0.020	1.2	0.47	5.04	1.1	0.322	1.07	0.985	0.114	0.188	1797	17	1859	3	3.3
2.1	Grt,eq	3875	25021	6.7	1051	4.9E-4	5	0.846	2.3	0.48	4.88	1.2	0.316	1.14	0.940	0.112	0.414	1769	18	1834	7	3.5
2.1.2	Grt,eq	4152	27642	6.9	1150	1.7E-4	11	0.287	2.3	0.38	5.05	1.1	0.322	1.09	0.952	0.114	0.351	1801	17	1857	6	3.0
3.1	Grt,eq	9781	25923	2.7	2702	1.4E-5	49	0.025	0.8	0.50	5.06	1.1	0.322	1.09	0.976	0.114	0.242	1797	17	1867	4	3.7
3.1.2	Grt,eq	12913	33871	2.7	4108	1.3E-5	86	0.022	0.9	0.59	5.79	1.2	0.370	1.12	0.965	0.113	0.305	2031	19	1855	6	-9.5
4.1	Grt,eq	8949	16622	1.9	2386	2.0E-4	6	0.343	0.6	1.11	4.90	1.1	0.310	1.10	0.968	0.114	0.284	1743	17	1870	5	6.8
47.1	mat,S2,lt	1367	28432	21.5	354	4.0E-4	9	0.685	6.5	0.54	4.46	1.3	0.302	1.16	0.892	0.107	0.588	1701	17	1752	11	2.9
47.2	mat,S2,lt	3460	33850	10.1	954	2.6E-5	35	0.045	3.0	0.30	4.99	1.1	0.321	1.10	0.974	0.113	0.257	1795	17	1843	5	2.6
09SRB-C49 - z10221 (UTM zone 20; 439515E 7296221N) - IP556																						
136.1	mat,S2	4241	22046	5.4	1129	1.8E-5	52	0.032	1.7	0.32	4.85	1.1	0.310	1.06	0.978	0.113	0.226	1740	16	1855	4	6.2
136.2	mat,S2	5303	18816	3.7	1424	1.7E-5	42	0.030	1.1	0.39	4.91	1.1	0.313	1.07	0.980	0.114	0.218	1754	16	1863	4	5.9
136.3	mat,S2	5098	26222	5.3	1367	2.5E-5	26	0.043	1.6	0.33	4.89	1.1	0.312	1.06	0.981	0.114	0.211	1751	16	1859	4	5.8
135.1	mat,S2,r	5145	27124	5.4	1405	2.5E-5	35	0.043	1.7	0.70	4.92	1.1	0.318	1.06	0.982	0.112	0.205	1779	16	1835	4	3.0
135.2	mat,S2	3058	39052	13.2	856	3.4E-5	46	0.060	4.0	0.28	5.14	1.1	0.326	1.08	0.963	0.114	0.302	1818	17	1869	5	2.7
135.3	mat,S2	4736	30345	6.6	1313	4.1E-5	23	0.070	1.9	0.36	5.05	1.1	0.323	1.08	0.972	0.114	0.261	1803	17	1857	5	2.9
135.4	mat,S2,r	7464	31069	4.3	2003	1.1E-5	97	0.018	1.3	0.33	4.79	1.1	0.312	1.10	0.981	0.111	0.220	1752	17	1818	4	3.6
107.1	mat,S2	4046	29734	7.6	1164	1.6E-5	53	0.028	2.2	0.33	5.25	1.1	0.335	1.08	0.976	0.114	0.243	1862	18	1860	4	-0.1
107.2	mat,S2	7055	29601	4.3	2006	5.1E-6	111	0.009	1.3	0.32	5.16	1.1	0.331	1.06	0.985	0.113	0.184	1843	17	1849	3	0.3
107.3	mat,S2	3687	39560	11.1	1084	3.7E-5	22	0.065	3.4	0.37	5.38	1.1	0.342	1.08	0.977	0.114	0.235	1897	18	1865	4	-1.7
107.4	mat,S2	5441	46598	8.8	1596	2.0E-5	26	0.035	2.6	0.29	5.42	1.1	0.341	1.07	0.982	0.115	0.208	1894	18	1880	4	-0.7

Notes (*see* Stern and Berman, 2000; Stern and Sanborn, 1998):

Spot name follows the convention x-y.z; where x = lab sample number, y = grain number and z = spot number. Multiple analyses in an individual spot are labelled as x-y.z.z

Location (Mnz textural location): mat = matrix grain; St, And, Grt = inclusions in St ,And, Grt; $S_2(S_1)$ = aligned with $S_2(S_1)$; xS_2 = high angle to S_2; Sil = hosts Sil inclusions; lt = late; eq = equant; fr = fractured; frf = fracture fill; r = rim.

Uncertainties reported at 1σ (absolute) and are calculated by numerical propagation of all known sources of error.

$f(206)^{204}$ refers to mole fraction of total ^{206}Pb that is due to common Pb, calculated using the ^{204}Pb-method; common Pb composition used is the surface blank (4/6: 0.05770; 7/6: 0.89500; 8/6: 2.13840).

* refers to radiogenic Pb (corrected for common Pb); Concordance relative to origin = 100 * (206/238 age)/($^{207}Pb/^{206}Pb$ age)

Calibration standard 8153; Age = 511.6 Ma; $^{206}Pb/^{238}U$ = 0.0826

Analytical details:

IP556: 9μm spot, 6 scans; error in $^{206}Pb/^{238}U$ calibration 1.03%; U concentration standard z8153, 2065 ppm; Th/U calibration: F = ThO/UO*0.85700

Mass fractionation correction = +0.9% was applied to the Pb-isotope ratios.

IP615: 12μm spot, 6 scans; error in $^{206}Pb/^{238}U$ calibration 1.23%; U concentration standard z8153, 2065 ppm. Th/U :F = ($^{208}Pb^{*}/^{206}Pb^{*}$)/(ThO/UO))/0.2888

No mass fractionation correction was applied.

Table 2. (Cont.)

Spot	Location	U (ppm)	Th (ppm)	Th/U	$^{206}Pb^*$ (ppm)	$^{204}Pb/^{206}Pb$	% ±	$f(206)^{204}$ (%)	$^{208*}Pb/^{206*}Pb$	% ±	$^{207*}Pb/^{235}U$	% ±	$^{206*}Pb/^{238}U$	% ±	Corr Coeff	$^{207*}Pb/^{206*}Pb$	% ±	Apparent Ages (Ma) $^{206}Pb/^{238}U$	± $^{206}Pb/^{238}U$	$^{207}Pb/^{206}Pb$	± $^{207}Pb/^{206}Pb$	Disc. (%)
09SRB-M82 - z10216 (UTM zone 20; 484751E 7320160N) - IP556																						
89.1.1	mat,S2	2164	17586	8.4	595	5.9E-5	22	0.101	2.5	0.35	5.03	1.1	0.320	1.11	0.965	0.114	0.299	1789	17	1864	5	4.0
89.1.2	mat,S2	2591	21473	8.6	693	2.9E-5	71	0.051	2.6	0.38	4.87	1.2	0.311	1.11	0.948	0.114	0.373	1747	17	1858	7	6.0
89.1.3	mat,S2	3237	27091	8.6	875	4.6E-5	31	0.079	2.6	0.41	4.98	1.2	0.315	1.12	0.956	0.115	0.344	1764	17	1875	6	5.9
89.1.4	mat,S2	3858	33457	9.0	1052	4.1E-5	33	0.070	2.7	0.44	4.98	1.2	0.317	1.16	0.953	0.114	0.369	1777	18	1861	7	4.5
90.1	mat,S2	2531	27563	11.2	716	8.2E-5	19	0.142	3.5	0.32	5.17	1.2	0.329	1.11	0.959	0.114	0.325	1834	18	1863	6	1.5
90.2	mat,S2	5946	58675	10.2	1735	4.4E-5	18	0.075	3.0	0.25	5.33	1.1	0.340	1.07	0.982	0.114	0.208	1885	17	1861	4	-1.3
91.1	mat,S2	2805	36106	13.3	794	4.7E-5	28	0.081	4.0	0.32	5.17	1.2	0.330	1.12	0.962	0.114	0.317	1836	18	1861	6	1.3
91.2	mat,S2	2575	37451	15.0	723	9.6E-5	18	0.166	4.4	0.33	5.08	1.3	0.327	1.20	0.956	0.113	0.367	1822	19	1845	7	1.3
91.3	mat,S2	12533	20314	1.7	3530	8.1E-6	62	0.014	0.5	0.47	5.16	1.1	0.328	1.06	0.987	0.114	0.169	1828	17	1866	3	2.0
37.1	St,S2	3186	19889	6.4	903	1.6E-4	21	0.274	1.8	0.37	5.18	1.2	0.330	1.09	0.919	0.114	0.471	1838	17	1863	8	1.3
37.2	St,S2	3143	21562	7.1	860	5.0E-5	28	0.087	2.1	0.38	5.01	1.1	0.319	1.10	0.963	0.114	0.305	1783	17	1864	6	4.4
86.1	mat ,xS2	6930	6052	0.9	1908	7.6E-6	68	0.013	0.3	0.57	5.03	1.1	0.321	1.06	0.988	0.114	0.163	1792	17	1862	3	3.7
86.2	mat ,xS2	3738	20998	5.8	1046	1.4E-5	49	0.024	1.6	0.37	5.14	1.3	0.326	1.28	0.983	0.114	0.237	1817	20	1870	4	2.8
86.3	mat ,xS2	8791	11474	1.3	2439	2.9E-5	18	0.050	0.4	0.51	5.06	1.1	0.323	1.06	0.988	0.114	0.167	1804	17	1859	3	2.9
49.1	mat ,xS2	2748	33930	12.8	782	5.9E-5	21	0.103	3.8	0.28	5.14	1.1	0.331	1.09	0.969	0.113	0.278	1845	18	1841	5	-0.2
49.2	mat ,xS2	2770	36601	13.7	794	1.4E-4	21	0.238	4.0	0.31	5.17	1.2	0.334	1.10	0.927	0.112	0.446	1856	18	1839	8	-0.9
10SRB-M240 - z10590 (UTM zone 20; 531935E 7370690N) - IP615																						
11.1	And,S1	2440	30726	13.0	678	8.9E-5	31	0.155	3.68	0.68	5.16	1.6	0.324	1.51	0.921	0.116	0.6	1807	24	1891	11	5.1
11.1.2	And,S1	1946	26379	14.0	539	5.8E-5	24	0.100	4.02	0.49	5.15	1.4	0.322	1.36	0.958	0.116	0.4	1801	21	1896	7	5.7
11.2	And,S1	2405	29559	12.7	738	6.0E-5	52	0.104	3.71	0.40	5.74	1.5	0.357	1.40	0.925	0.116	0.6	1970	24	1903	10	-4.1
11.2.2	And,S1	2567	31329	12.6	706	5.6E-5	30	0.098	3.59	0.39	5.10	1.5	0.320	1.40	0.947	0.115	0.5	1791	22	1887	9	5.8
13.1	And,S1	1779	17108	9.9	499	5.0E-5	31	0.087	2.81	0.43	5.17	1.5	0.327	1.41	0.948	0.115	0.5	1822	22	1876	9	3.3
13.1.2	And,S1	1719	15969	9.6	451	3.7E-5	76	0.063	2.78	0.51	4.85	1.5	0.305	1.42	0.929	0.115	0.6	1717	21	1884	10	10.1
196.1	Grt	1655	17012	10.6	471	3.3E-4	11	0.574	3.01	0.63	5.32	1.7	0.332	1.49	0.903	0.116	0.7	1847	24	1899	13	3.2
196.1.2	Grt	1751	17833	10.5	444	4.8E-4	10	0.833	3.01	0.52	4.72	1.8	0.295	1.63	0.897	0.116	0.8	1667	24	1896	14	13.7
35.1	mat,late	2284	14566	6.6	597	2.5E-4	17	0.428	2.00	1.50	4.67	1.9	0.304	1.72	0.911	0.111	0.8	1712	26	1821	14	6.8
35.1.2	mat,late	2255	15633	7.2	573	1.6E-4	16	0.277	2.06	0.72	4.41	1.7	0.296	1.52	0.914	0.108	0.7	1671	22	1769	12	6.3
38.1	mat,late,r	2256	21239	9.7	593	3.9E-4	9	0.676	2.74	0.45	4.57	1.6	0.306	1.42	0.909	0.108	0.7	1722	21	1770	12	3.1
38.2	mat,late	2026	15571	7.9	580	2.9E-5	54	0.051	2.23	0.53	5.05	2.0	0.333	1.90	0.960	0.110	0.6	1855	31	1798	10	-3.7
38.2.2	mat,late	2229	18998	8.8	550	2.4E-5	64	0.042	2.43	0.52	4.39	1.6	0.287	1.45	0.935	0.111	0.6	1629	21	1813	10	11.5
183.1	mat,late,Sil	3656	19476	5.5	986	1.1E-4	14	0.194	1.54	0.46	4.76	1.5	0.314	1.42	0.958	0.110	0.4	1761	22	1797	8	2.3
183.2	mat,late,Sil	4394	23158	5.4	1247	6.6E-5	19	0.115	1.57	0.41	5.03	1.4	0.330	1.34	0.964	0.111	0.4	1841	21	1808	7	-2.1
214.1	mat,fr	1743	22263	13.2	454	1.9E-4	24	0.323	3.81	0.39	4.61	1.6	0.303	1.41	0.893	0.110	0.7	1707	21	1804	13	6.1
214.2	mat,fr,r	2169	21101	10.0	558	6.8E-5	30	0.118	2.88	0.48	4.47	1.6	0.299	1.44	0.931	0.108	0.6	1689	21	1772	10	5.3
252.1	Grt,fr	4716	25390	5.6	1265	2.5E-5	32	0.043	1.58	0.47	4.77	1.4	0.312	1.35	0.961	0.111	0.4	1752	21	1813	7	3.8
252.1.2	Grt,fr	4441	22241	5.2	1175	1.9E-5	50	0.033	1.50	0.51	4.66	1.4	0.308	1.36	0.954	0.110	0.4	1731	21	1794	8	4.1
252.2	Grt,fr	3039	20503	7.0	796	7.0E-5	20	0.121	2.01	0.65	4.61	1.6	0.305	1.49	0.922	0.110	0.6	1715	22	1795	11	5.0
252.2.2	Grt,fr	3498	22935	6.8	906	1.9E-5	68	0.032	1.94	0.76	4.60	1.4	0.302	1.33	0.957	0.111	0.4	1699	20	1811	7	7.0
252.3	Grt,fr	1442	19088	13.7	394	3.1E-4	11	0.536	4.08	0.49	4.78	1.6	0.319	1.43	0.910	0.109	0.6	1782	22	1780	12	-0.2
252.3.2	Grt,fr	1699	18903	11.5	426	6.0E-5	35	0.104	3.39	0.53	4.36	1.7	0.292	1.49	0.888	0.109	0.8	1650	22	1775	14	8.0
283.1	Grt,fr	1635	28009	17.7	439	1.5E-4	17	0.268	5.10	0.39	4.77	1.6	0.312	1.44	0.925	0.111	0.6	1751	22	1814	11	4.0
283.1.2	Grt,fr	1533	26073	17.6	370	1.0E-4	24	0.178	4.94	0.41	4.30	1.8	0.281	1.73	0.945	0.111	0.6	1597	25	1816	11	13.6
285.1	mat,S2,fr	2217	19533	9.1	568	5.4E-4	10	0.937	2.56	0.61	4.57	1.9	0.299	1.57	0.821	0.111	1.1	1684	23	1817	20	8.3
34.1	And,fr	2013	19522	10.0	523	1.4E-4	18	0.236	2.91	0.52	4.54	2.0	0.302	1.94	0.962	0.109	0.6	1703	29	1783	10	5.1
34.1.2	And,fr	2072	19771	9.9	512	1.2E-4	18	0.213	2.80	0.46	4.39	1.5	0.288	1.42	0.933	0.111	0.5	1630	20	1810	10	11.2
36.1	mat,S2,fr	1533	11909	8.0	414	3.2E-4	11	0.552	2.31	0.53	4.73	1.6	0.315	1.46	0.903	0.109	0.7	1763	23	1782	13	1.2
194.1	Grt,fr	1285	16118	13.0	363	6.6E-4	11	1.145	3.71	0.69	5.12	2.2	0.329	1.81	0.829	0.113	1.2	1834	29	1843	22	0.6
197.1	Grt,fr	1721	37293	22.4	485	3.6E-4	13	0.629	6.54	0.41	5.19	2.9	0.328	2.63	0.920	0.115	1.1	1830	42	1875	20	2.8
197.1.2	Grt,fr	1567	36436	24.0	417	2.7E-4	18	0.462	6.92	1.06	4.86	1.7	0.309	1.51	0.880	0.114	0.8	1738	23	1862	15	7.6
195.1	Grt,frf	833	23695	29.4	212	1.2E-3	9	2.109	8.84	0.53	4.26	2.4	0.296	1.74	0.713	0.105	1.7	1669	26	1706	31	2.5
195.1.2	Grt,frf	757	21507	29.4	197	6.4E-4	12	1.105	8.54	0.65	4.45	2.2	0.302	1.71	0.791	0.107	1.3	1704	26	1744	24	2.7

Table 2. (Cont.)

Spot	Location	U (ppm)	Th (ppm)	Th/U	$^{206}Pb^*$ (ppm)	$^{204}Pb/^{206}Pb$	% ±	$f(206)^{204}$ (%)	$^{208*}Pb/^{206*}Pb$	% ±	$^{207*}Pb/^{235}U$	% ±	$^{206*}Pb/^{238}U$	% ±	Corr Coeff	$^{207*}Pb/^{206*}Pb$	% ±	Apparent Ages (Ma) $^{206}Pb/^{238}U$	$\pm^{206}Pb/^{238}U$	$^{207}Pb/^{206}Pb$	$\pm^{207}Pb/^{206}Pb$	Disc. (%)
10SRB-G14 - z10591 (UTM zone 20; 466069E 7406719N) - IP615																						
34.1	mat,S2,fr	6280	35103	5.8	1757	3.7E-5	15	0.064	1.67	0.31	4.97	1.3	0.326	1.29	0.980	0.111	0.3	1817	20	1811	5	-0.4
81.2	mat,late	6374	37967	6.2	1801	3.9E-5	20	0.067	1.80	0.36	5.08	1.6	0.329	1.56	0.981	0.112	0.3	1833	25	*1832*	6	-0.1
112.1	mat,S2,r	9684	31690	3.4	2686	5.1E-5	19	0.089	0.98	0.67	4.99	1.4	0.323	1.32	0.946	0.112	0.5	1804	21	*1832*	8	1.8
192.1	mat,S2,r	7468	36617	5.1	2035	3.5E-5	14	0.060	1.48	0.28	4.90	1.3	0.317	1.27	0.986	0.112	0.2	1777	20	*1834*	4	3.6
35.4.2	mat,S2,fr	8114	31812	4.0	2062	1.3E-5	31	0.022	1.17	0.38	4.58	1.3	0.296	1.27	0.986	0.112	0.2	1670	19	*1837*	4	10.3
82.2.2	mat,S2,r	5970	39121	6.8	1609	1.2E-5	35	0.021	1.93	0.39	4.87	1.4	0.314	1.32	0.970	0.113	0.3	1759	20	*1841*	6	5.1
35.2.2	mat,S2,fr	8725	42773	5.1	2555	9.2E-6	31	0.016	1.42	0.45	5.29	1.4	0.341	1.32	0.969	0.113	0.3	1891	22	*1842*	6	-3.1
35.4	mat,S2,fr	9101	34589	3.9	2482	9.2E-6	58	0.016	1.10	0.67	4.93	1.4	0.317	1.32	0.977	0.113	0.3	1777	21	*1842*	5	4.0
35.2	mat,S2,fr	9018	41830	4.8	2695	1.4E-5	30	0.025	1.35	0.41	5.40	1.3	0.348	1.31	0.973	0.113	0.3	1924	22	*1842*	6	-5.2
33.1	mat,S2,fr	6679	35603	5.5	1969	3.0E-5	19	0.053	1.55	0.41	5.33	1.4	0.343	1.32	0.946	0.113	0.5	1902	22	*1844*	8	-3.7
82.1	mat,S2,r	4920	40140	8.4	1394	3.3E-5	38	0.057	2.43	0.29	5.13	1.3	0.330	1.30	0.973	0.113	0.3	1837	21	*1844*	6	0.4
35.3.2	mat,S2,fr	8816	38954	4.6	2732	8.0E-6	26	0.014	1.34	0.43	5.61	1.6	0.361	1.62	0.981	0.113	0.3	1986	28	*1846*	6	-8.8
190.1	mat,eq	9489	35992	3.9	2767	3.4E-5	18	0.058	1.12	0.41	5.29	1.3	0.339	1.30	0.978	0.113	0.3	1884	21	1848	5	-2.3
191.1	mat,eq	4695	34837	7.7	1290	2.4E-5	24	0.041	2.24	0.98	4.98	2.6	0.320	2.53	0.970	0.113	0.6	1789	40	1848	11	3.6
112.4.2	mat,S2	12284	37966	3.2	3425	7.1E-6	48	0.012	0.90	0.32	5.06	1.3	0.325	1.27	0.988	0.113	0.2	1812	20	1849	4	2.3
81.2.2	mat,lt	5939	35421	6.2	1559	6.0E-6	48	0.010	1.81	0.41	4.76	1.4	0.306	1.34	0.969	0.113	0.3	1719	20	*1849*	6	8.1
72.1	Grt,S2	11200	36958	3.4	3171	1.6E-5	19	0.028	0.97	0.29	5.14	1.4	0.330	1.34	0.991	0.113	0.2	1837	21	1850	3	0.8
112.4	mat,S2,fr	11272	35064	3.2	3222	1.4E-5	23	0.025	0.92	0.33	5.19	1.3	0.333	1.28	0.987	0.113	0.2	1852	21	1850	4	-0.1
72.1.2	Grt,S2	11503	38169	3.4	3021	2.1E-5	26	0.036	0.99	0.31	4.77	1.3	0.306	1.27	0.987	0.113	0.2	1720	19	1851	4	8.1
80.1.2	Grt	5418	37917	7.2	1420	1.9E-5	28	0.033	2.10	0.51	4.76	1.3	0.305	1.29	0.981	0.113	0.3	1717	19	1851	5	8.2
71.1.2	Grt,S2	5121	25007	5.0	1351	2.1E-5	40	0.037	1.52	0.39	4.80	1.4	0.307	1.31	0.970	0.113	0.3	1727	20	1854	6	7.8
71.1	Grt,S2,Sil	6313	33990	5.6	1723	5.3E-5	19	0.092	1.59	0.30	4.97	1.3	0.318	1.32	0.980	0.113	0.3	1779	21	1855	5	4.7
80.1	Grt,S2	5887	37302	6.5	1592	3.1E-5	18	0.054	1.92	0.41	4.93	1.3	0.315	1.31	0.978	0.113	0.3	1765	20	1856	5	5.6
82.2	mat,S2	5933	39536	6.9	1702	6.8E-6	89	0.012	1.96	0.34	5.22	1.3	0.334	1.31	0.975	0.113	0.3	1857	21	1856	5	-0.1
35.1	mat,S2	8264	30516	3.8	2294	2.4E-5	32	0.042	1.12	0.33	5.06	1.3	0.323	1.28	0.983	0.114	0.2	1805	20	1857	4	3.2
125.1	Grt,S2	4049	32772	8.4	1127	6.1E-5	16	0.105	2.41	0.32	5.07	1.4	0.324	1.32	0.973	0.114	0.3	1809	21	1858	6	3.0
112.2.2	mat,S2	5907	35279	6.2	1587	1.2E-5	36	0.021	1.76	0.42	4.90	1.4	0.313	1.33	0.933	0.114	0.5	1754	20	1860	9	6.5
191.1.3	mat,eq	4272	30233	7.3	1117	3.0E-5	26	0.052	2.15	0.33	4.78	1.4	0.304	1.34	0.947	0.114	0.5	1713	20	1863	8	9.1
190.1.2	mat,eq	7386	30163	4.2	2038	4.4E-5	22	0.076	1.21	1.57	5.05	2.0	0.321	1.97	0.989	0.114	0.3	1796	31	1864	5	4.2
191.1.2	mat,eq	4688	33673	7.4	1326	5.0E-5	19	0.086	2.17	0.34	5.19	1.4	0.329	1.32	0.971	0.114	0.3	1835	21	1869	6	2.1
112.3	mat,S2	3812	36079	9.8	1082	7.0E-5	19	0.122	2.87	0.39	5.22	1.4	0.331	1.36	0.956	0.114	0.4	1841	22	1872	8	1.9
112.2	mat,S2	5778	38626	6.9	1697	4.1E-5	23	0.071	2.00	0.44	5.40	1.4	0.342	1.36	0.972	0.115	0.3	1896	22	1873	6	-1.5
112.3.2	mat,S2	3768	37580	10.3	1055	4.0E-5	28	0.069	3.09	0.34	5.15	1.4	0.326	1.33	0.964	0.115	0.4	1819	21	1874	7	3.4

Notes (*see* Stern and Berman, 2000; Stern and Sanborn, 1998):

Spot name follows the convention x-y.z; where x = lab sample number, y = grain number and z = spot number. Multiple analyses in an individual spot are labelled as x-y.z.z

Location (Mnz textural location): mat = matrix grain; St, And, Grt = inclusions in St ,And, Grt; $S_2(S_1)$ = aligned with $S_2(S_1)$; xS_2 = high angle to S_2; Sil = hosts Sil inclusions; lt = late; eq = equant; fr = fractured; frf = fracture fill; r = rim.

Uncertainties reported at 1σ (absolute) and are calculated by numerical propagation of all known sources of error.

$f(206)^{204}$ refers to mole fraction of total ^{206}Pb that is due to common Pb, calculated using the ^{204}Pb-method; common Pb composition used is the surface blank (4/6: 0.05770; 7/6: 0.89500; 8/6: 2.13840).

* refers to radiogenic Pb (corrected for common Pb); Concordance relative to origin = 100 * (206/238 age)/($^{207}Pb/^{206}Pb$ age)

Calibration standard 8153; Age = 511.6 Ma; $^{206}Pb/^{238}U$ = 0.0826

Analytical details:

IP556: 9μm spot, 6 scans; error in $^{206}Pb/^{238}U$ calibration 1.03%; U concentration standard z8153, 2065 ppm; Th/U calibration: F = ThO/UO*0.85700

Mass fractionation correction = +0.9% was applied to the Pb-isotope ratios.

IP615: 12μm spot, 6 scans; error in $^{206}Pb/^{238}U$ calibration 1.23%; U concentration standard z8153, 2065 ppm. Th/U :F = ($^{208}Pb^*/^{206}Pb^*$)/(ThO/UO))/0.2888

No mass fractionation correction was applied.

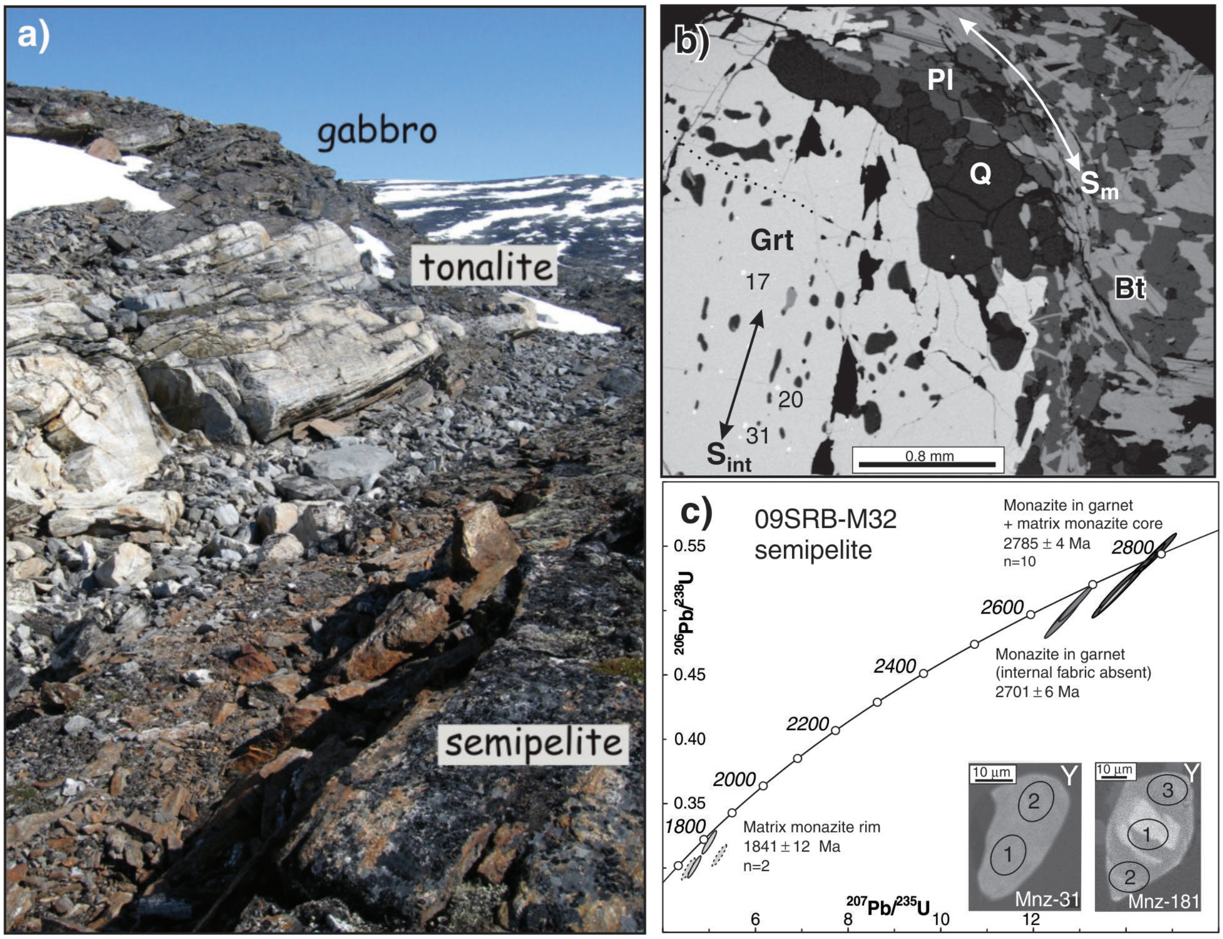

Figure 3. Semipelite M32. **a)** View to east of light grey-weathering tonalite basement complex containing structurally low panel of rust-weathering semipelite and structurally high panel of dark-weathering gabbro. 2013-029. **b)** Backscattered electron (BSE) image of garnet porphyroblast with internal foliation (S_{int}) enveloped by main matrix foliation (S_m). Dotted line shows textural break between low-Ca core with quartz inclusion fabric (S_{int}) and high-Ca rim with quartz inclusions at a high angle to S_{int}; numbers in Grt core identify monazite grains analyzed; mineral abbreviations: Q = quartz; Bt = biotite, Grt = garnet, Pl = plagioclase. **c)** Concordia diagram of SHRIMP U-Pb results for M32. Confidence ellipses and weighted mean $^{207}Pb/^{206}Pb$ ages are presented at the 95% confidence interval. Monazites within garnet are shown in medium and dark grey. Matrix monazites are shown in light grey. Analyses excluded from the calculation of weighted mean ages are drawn using a dashed outline. Insets show yttrium X-ray maps of monazite (Mnz) #31 and #181.

internal fabric is not present in most porphyroblasts, although several host a biotite-sillimanite-quartz fabric that is oblique to, or parallels, the main foliation. A 1.5 mm by 2 mm garnet porphyroblast shows very little compositional zonation (X_{Grs} = 0.039–0.042; Fe/(Fe+Mg) = 0.78–0.79; X_{Sps} = 0.02), except at rims touching biotite (Fe/(Fe+Mg) = 0.82). Approximate P-T conditions of 6 kbar and 700°C are in good agreement with calculated phase relationships and garnet compositions.

A mean $^{207}Pb/^{206}Pb$ age of 1897 ± 8 Ma (MSWD = 0.61) was determined from two SHRIMP analyses of the high-Y core of a slightly elongate monazite inclusion (#14) associated with randomly oriented sillimanite within a subequant garnet porphyroblast (Fig. 4b). Eight analyses of two foliation-parallel matrix grains (e.g. #16 in Fig. 4b) give a weighted mean age of 1862 ± 12 Ma with some excess scatter (MSWD = 2.3).

09SRB-H108 (GSC lab number 10219)

Semipelite H108, and associated marble and chert, are interpreted to be part of the Paleoproterozoic cover sequence, infolded with Archean tonalitic basement on the southern limb of an upright F_2 synform (Fig. 2). At this location, 10 m wide gabbro sills alternate with the garnet-biotite-sillimanite-plagioclase-quartz semipelite with quartz+plagioclase leucosomes (Fig. 5a). The unusual abundance of gabbro sills

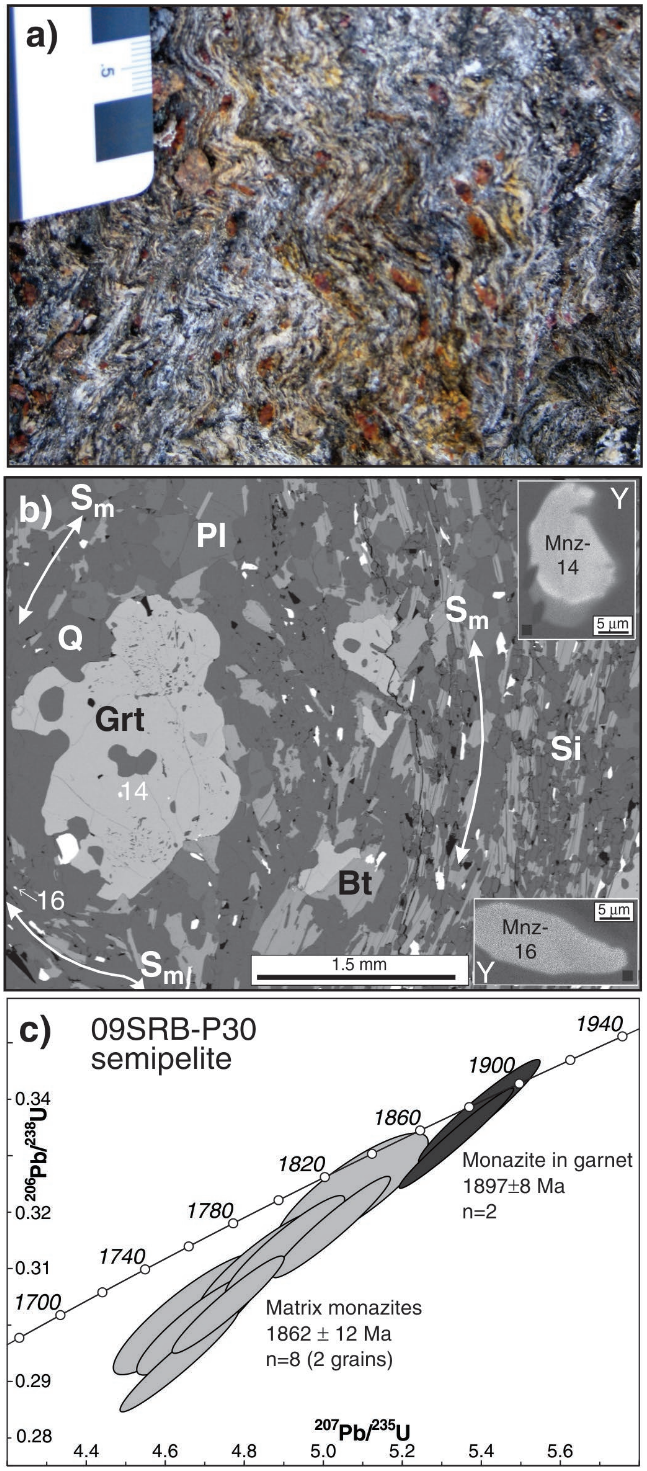

Figure 4. Semipelite P30. **a)** Crenulated biotite-sillimanite±garnet foliation. 2013-027. **b)** BSE image showing main foliation (S_m) enveloping garnet porphyroblast with internal randomly oriented sillimanite needles. Numbers identify monazite grains analyzed; insets show yttrium X-ray maps of these monazite grains; Mineral abbreviations as in Figure 3, with Si = sillimanite. **c)** Concordia diagram of SHRIMP U-Pb results. Confidence ellipses and weighted mean $^{207}Pb/^{206}Pb$ ages are presented at the 95% confidence interval. Monazite within garnet is shown in dark grey. Matrix monazites are shown in light grey.

at this location, potentially feeders to overlying volcanic rocks, highlights a significant magmatic thermal input at this locality.

Biotite, sillimanite, and leucosome define a strong $L_2 \geq S_2$ fabric (S_2 = 279/20, L_2 = 080/07), which is typical of the north-dipping, shallow-plunging structures that characterize this south-vergent fold and thrust belt. Biotite and sillimanite wrap equant to subequant garnet porphyroblasts that are up to 1 cm in diameter. Larger garnet porphyroblasts have a weak internal fabric defined by some combination of elongate quartz (Fig. 5b), ilmenite, biotite, staurolite, and plagioclase. The included garnet fabrics are approximately straight and usually at a high angle to the external fabric. A garnet porphyroblast approximately 11 mm in diameter has a chemically homogeneous core with Mn- and Fe-enriched rims.

A mean $^{207}Pb/^{206}Pb$ age of 1881 ± 8 Ma (MSWD = 0.18) was derived from three SHRIMP analyses (Fig. 5c) of a slightly elongate monazite inclusion (#291) that parallels a weak quartz inclusion fabric within garnet (Fig. 5b). Three analyses of the core of a highly elongate, foliation-parallel matrix grain (#527; Fig. 5b inset) yield an imprecise age of 1864 ± 27 Ma (MSWD = 7.8). The large excess scatter suggests mixing of different age domains, which may include a ca. 1880 Ma domain as well as a 1830–1813 Ma domain implied by analyses #527.2 and 527.4 nearest to the wide tip of this matrix grain. Further imaging of chemical domains in this grain is needed before the age results can be refined and interpreted with more confidence.

09SRB-H90 (GSC lab number 10218)

This strongly tectonized semipelitic gneiss, with gneissosity oriented 081/27°S, was collected from the north limb of a 3 km wide supracrustal enclave which forms a synformal F_2 fold within tonalite (Fig. 2). Associated silicate-facies iron-formation and ultramafic volcanic rocks suggest that these rocks are part of the Hoare Bay cover sequence. There is continuity in the orientation of S_2 from the sedimentary rocks structurally above to the mylonitic tonalite gneiss below, which establishes a tectonic contact with Archean basement at this location (Fig. 6a). The tonalite is characterized by south-verging, east-trending, outcrop-scale, recumbent F_2 folds.

The sample is a biotite-sillimanite-garnet-plagioclase-quartz migmatitic semipelite with leucosome composed of quartz and coarse plagioclase up to 8 mm in diameter. Subequant garnet porphyroblasts are 3 to 10 mm in diameter, and are wrapped by a biotite-sillimanite fabric. Many contain a weak, straight internal fabric (defined by elongate quartz, biotite, and ilmenite) oblique to the matrix foliation (Fig. 6b). A 4.5 mm diameter garnet porphyroblast has a homogeneous core, and a rimward increase in Mn and Fe/(Fe+Mg).

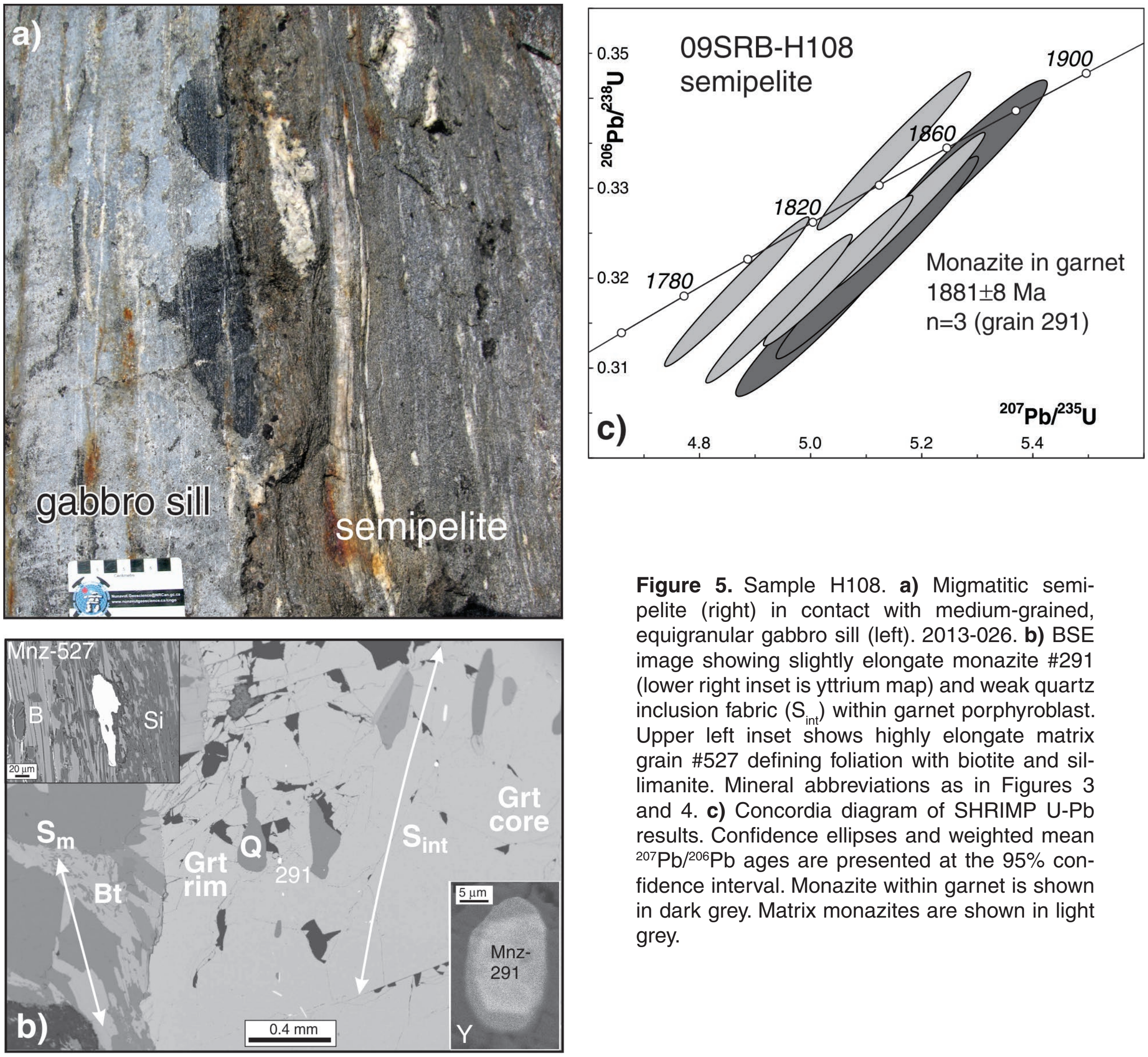

Figure 5. Sample H108. **a)** Migmatitic semipelite (right) in contact with medium-grained, equigranular gabbro sill (left). 2013-026. **b)** BSE image showing slightly elongate monazite #291 (lower right inset is yttrium map) and weak quartz inclusion fabric (S_{int}) within garnet porphyroblast. Upper left inset shows highly elongate matrix grain #527 defining foliation with biotite and sillimanite. Mineral abbreviations as in Figures 3 and 4. **c)** Concordia diagram of SHRIMP U-Pb results. Confidence ellipses and weighted mean ^{207}Pb/^{206}Pb ages are presented at the 95% confidence interval. Monazite within garnet is shown in dark grey. Matrix monazites are shown in light grey.

A weighted mean ^{207}Pb/^{206}Pb age of 1860 ± 5 Ma (MSWD = 1.16) was calculated from ten analyses (Fig. 6c) of five equant monazite inclusions (e.g. #137) within garnet porphyroblasts that contain a weak alignment of quartz and ilmenite inclusions at a high angle to the external foliation (Fig. 6b). A single spot age of 1834 Ma from monazite inclusion #2 was excluded as an outlier from this average. An irregular-shaped matrix grain (#47) with prismatic sillimanite inclusions and complex patchy zoning yields spot ages of 1843 Ma and 1750 Ma.

09SRB-C49 (GSC lab number 10221)

This sample of garnet-sillimanite-biotite-plagioclase-quartz pelite was collected from a rare exposure in a till-covered region located near tonalite dated at 2991 ± 4 Ma (Rayner et al., 2012). The foliation, defined by biotite, sillimanite, and the shape fabric of quartz and feldspar (Fig. 7a), strikes southwest (235°) with a variable (30–60°) northwest dip. Aligned sillimanite and tourmaline define a strong northwest-plunging mineral lineation.

Garnet porphyroblasts are up to 3 mm in diameter and enveloped by the foliation. A large porphyroblast contains a sigmoidal-shaped internal fabric (defined by elongate quartz and biotite) that is discontinuous with the external foliation. In some smaller garnet porphyroblasts, the internal fabric is continuous with the external foliation. A 3 mm garnet core is homogeneous, with a rim that has higher Fe and Mn.

A weighted mean ^{207}Pb/^{206}Pb age of 1859 ± 7 Ma (MSWD = 2.3, Fig. 7b) derives from eight analyses of 3 elongate matrix monazite grains that are parallel to the main foliation (e.g. Fig. 7a), with one outlying older, near-rim analysis (#107.4). Two near-rim analyses (#135.1, 135.4) of one of these grains gave spot ages of 1835 ± 8 Ma and 1818 ± 8 Ma.

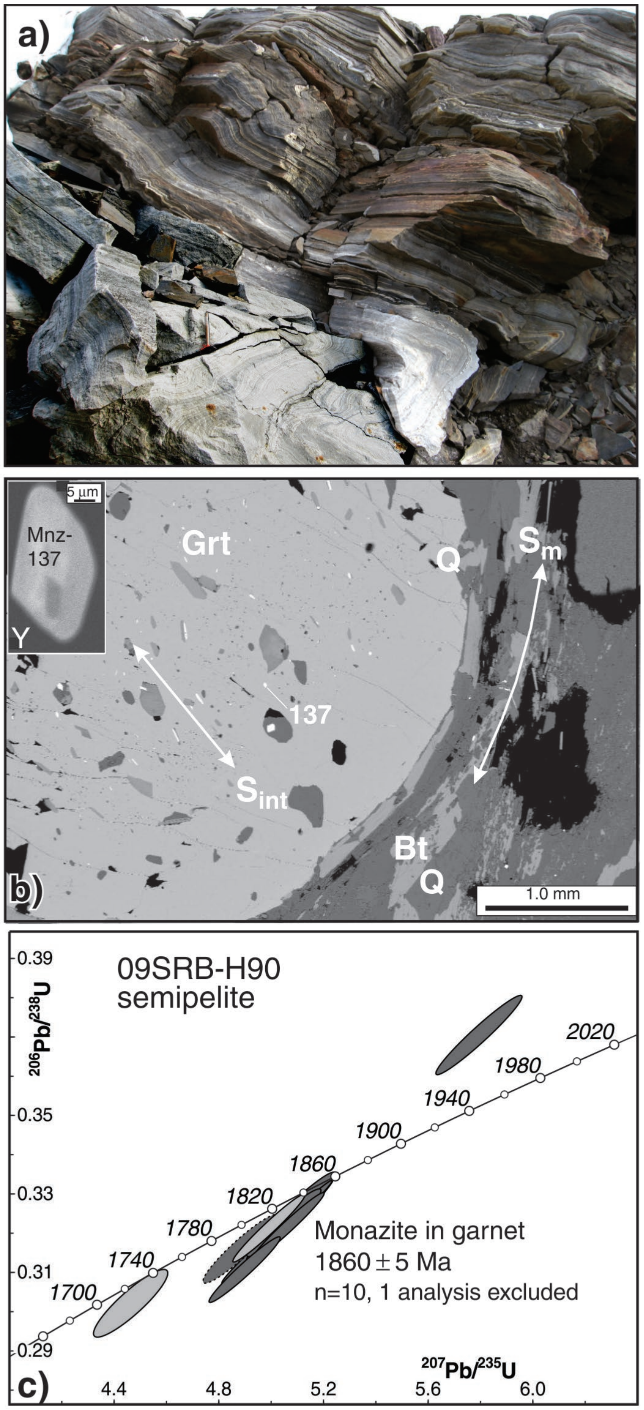

Figure 6. Locality H90. **a)** View to east of highly strained semipelitic paragneiss in contact with mylonitic orthogneiss. 2013-029. **b)** BSE image showing monazite inclusion #137 within large garnet porphyroblast with weak internal quartz and ilmenite inclusion fabric (S_{int}). Inset is yttrium X-ray map of this grain. Mineral abbreviations as in Figure 3. **c)** Concordia diagram of SHRIMP U-Pb results. Confidence ellipses and weighted mean $^{207}Pb/^{206}Pb$ ages are presented at the 95% confidence interval. Monazites within garnet are shown in dark grey. Analysis excluded from the calculation of weighted mean ages is drawn with a dashed outline. Matrix monazites are shown in light grey.

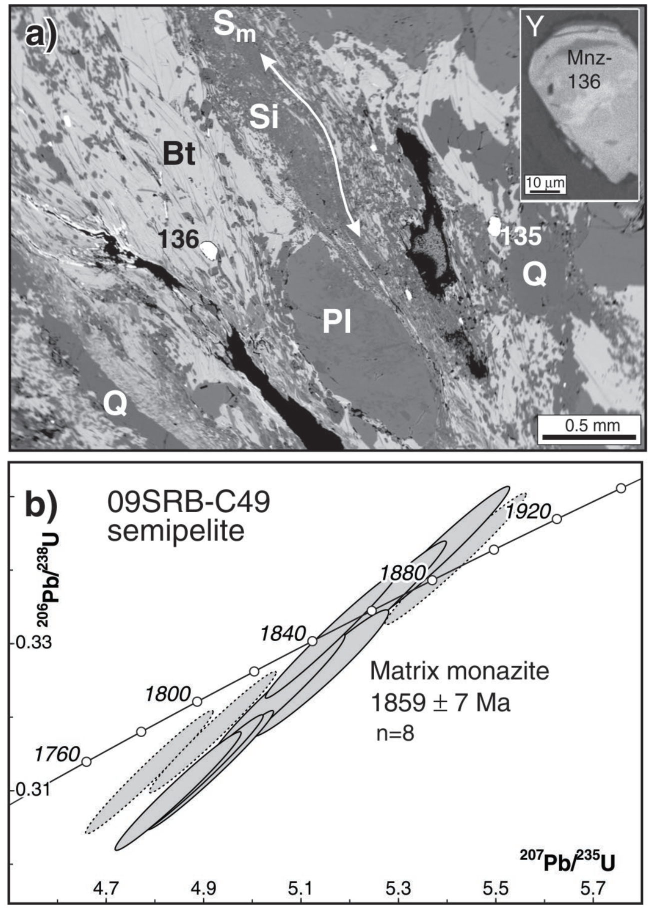

Figure 7. Sample C49. **a)** BSE image showing monazite grains #135 and 136 lying within strong penetrative foliation. Inset shows yttrium X-ray map of grain #136. Abbreviations as in Figure 3. **b)** Concordia diagram of SHRIMP U-Pb results. Confidence ellipses and weighted mean $^{207}Pb/^{206}Pb$ ages are presented at the 95% confidence interval. All analyzed monazites are from the matrix; analyses excluded from the calculation of weighted mean ages are drawn with a dashed outline.

09SRB-M82 (GSC lab number 10216)

This semipelitic sample was collected from the north-younging, southern limb of an upright, shallow-plunging F_2 syncline at one of the few exposures in the map area where primary stratigraphic features such as bedding, grading, parallel- and possible cross-stratification (Fig. 8a) are preserved. The sample was collected from a clastic section that is stratigraphically overlain by gossanous chert and ultramafic volcanic rocks, and hence correlative with the Totnes volcanic sequence (Keim et al., 2011). This sample, with its lower-amphibolite facies assemblage of garnet-staurolite-muscovite-biotite-plagioclase-quartz, is the lowest grade sample dated. It was collected from a low-grade domain referred to as the Touak-Sunneshine metamorphic low (Hamilton et al., 2012), a narrow 15 km by 125 km corridor of lower-amphibolite facies rocks that extends northeast from sample M82 (Fig. 2).

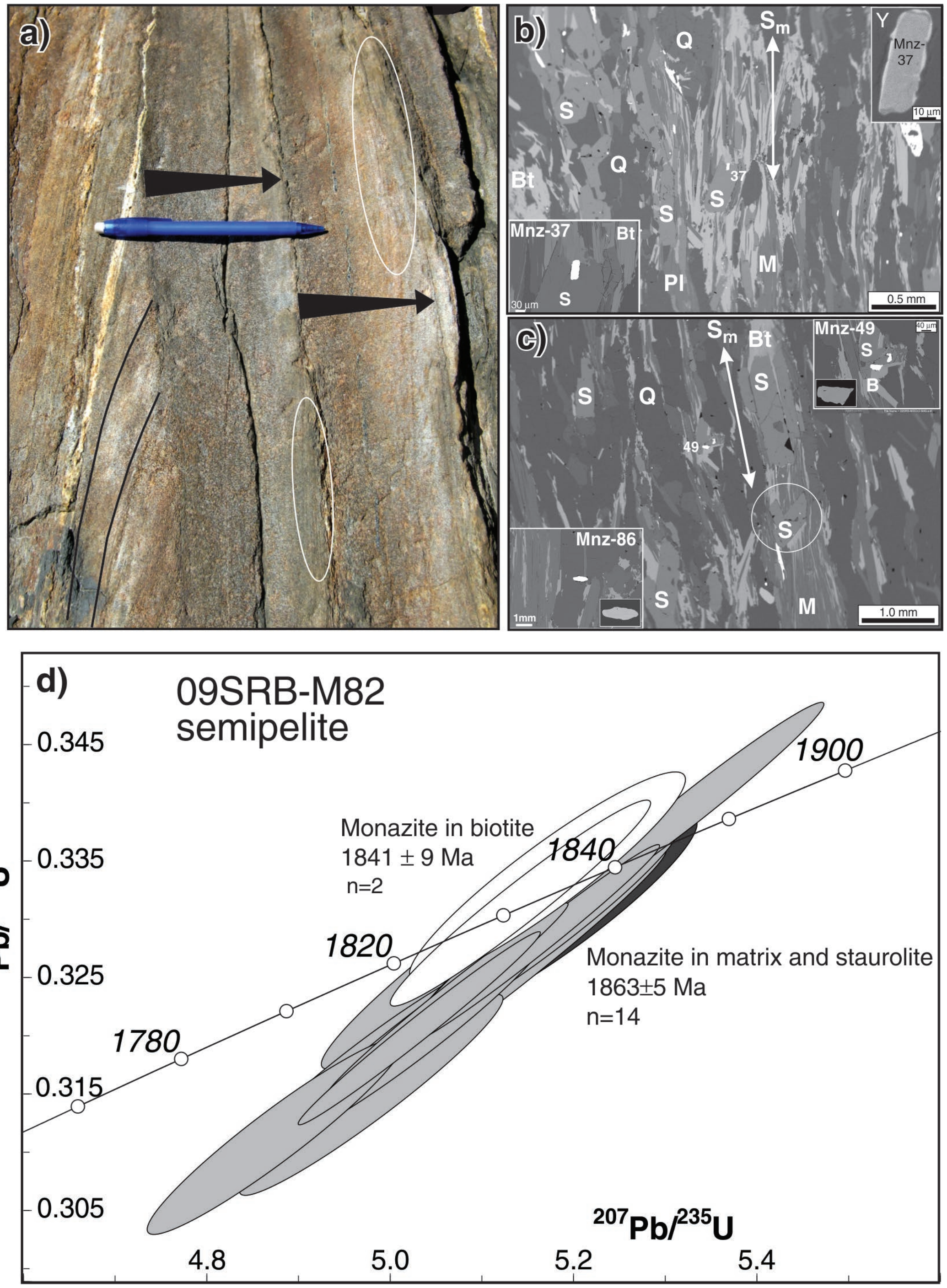

Figure 8. Locality M82. **a)** Horizontal exposure of steeply dipping limb of upright F_2 fold showing graded bedding (black arrows), parallel-laminated upper beds (white ellipses) and truncated cross-stratification (solid lines), all consistent with younging to the north (right). At this exposure, weak bedding-parallel S_1 is coplanar to axial planar S_2. 2013-028. **b)** BSE image of textural relationships in M82 showing main (S_1+S_2) foliation (S_m) defined by aligned biotite, muscovite (M), and staurolite (S); other abbreviations as in Figure 3. Insets show yttrium map and close-up of monazite (#37) partially included in staurolite. **c)** BSE image showing composite foliation (S_m) defined by muscovite, biotite, staurolite, and quartz with one euhedral staurolite crystal (circled white) appearing to have overgrown the foliation. Upper right inset shows close-up of BSE image and textural relationships of monazite #49. Lower left inset shows BSE image and textural setting of monazite #86 at a high angle to the foliation. **d)** Concordia diagram of SHRIMP U-Pb results. Confidence ellipses and weighted mean $^{207}Pb/^{206}Pb$ ages are presented at the 95% confidence interval. Analyses of one monazite mostly within staurolite are shown in dark grey, and matrix monazites are shown in light grey. Both are included in the calculation of the weighted mean age. White ellipses show two analyses of monazite #49, which is at high angle to the fabric.

The collected sample contains a steep composite fabric, defined by biotite and muscovite, wherein bedding-parallel S_1 is superimposed by axial planar S_2 oriented 078/80–90. Staurolite occurs as large porphyroblasts containing an internal quartz inclusion fabric at a high angle to the enveloping external foliation, and as smaller euhedral porphyroblasts lying within the foliation but cutting matrix biotite (Fig. 8b). In contrast, a few porphyroblasts cut across matrix biotite and muscovite (i.e. open circle in Fig. 8c). Accordingly, staurolite growth was predominantly pre- to syn-tectonic, but appears to have continued after deformation. Sparse sillimanite needles contribute to the S_2 foliation, particularly in regions surrounding garnet (this sample), and also are oriented randomly within matrix quartz (other, undated samples).

Garnet porphyroblasts up to 3 mm in diameter display an internal, sigmoidal to straight fabric at a high angle to, and discontinuous with the external, enveloping foliation. A 2 mm diameter garnet porphyroblast displays somewhat irregular growth zoning (rimward decrease in X_{Grs} and X_{Sps}) with Mn and Fe enriched rims interpreted to reflect garnet resorption. Most plagioclase is strongly zoned (e.g. core X_{An} = 0.37; rim X_{An} = 0.20). P-T data were not obtained because of the complexity of garnet and plagioclase zoning.

A weighted mean $^{207}Pb/^{206}Pb$ age of 1863 ± 5 Ma (MSWD = 1.4, Fig. 8d) derives from 14 analyses of four matrix monazite grains and a monazite mostly included in staurolite. Three of the matrix grains (#89, 90, 91) as well as the inclusion (#37) and its host staurolite (S in Fig. 8b) are elongate parallel to the foliation. Matrix monazite #86 is a somewhat scalloped, elongate grain oriented parallel to a set of discontinuous, foliation-perpendicular fractures within a large quartz crystal (Fig. 8c). An age of 1841 ± 9 Ma (MSWD = 0.04) results from two analyses of a monazite grain (#49) that crystallized between texturally late biotite and staurolite (Fig. 8c).

10SRB-M240 (GSC lab number 10590)

This metapelitic garnet-andalusite-staurolite-muscovite sample was collected from the limb of a metre-scale F_2 fold (e.g. Fig. 9a) on the north shore of Totnes Road, Exeter Sound in a similar stratigraphic position as M82. The sample contains large (~4–10 mm diameter) porphyroblasts of andalusite that define bedding-parallel S_1 (Fig. 9a,b) as well as a discrete axial planar S_2 foliation (Fig. 9b), which is oriented 254/72°N. Smaller (<1 mm) staurolite and andalusite crystals have unclear relationships to the foliation. A 5 mm diameter garnet porphyroblast decreases in CaO and MnO from core (X_{Grs} = 0.08; X_{Sps} = 0.25) to rim (X_{Grs} = 0.04; X_{Sps} = 0.19), consistent with growth zoning. Slightly higher Fe/(Fe+Mg) rims (0.86) than the core (0.85) suggest some modification via diffusional re-equilibration. Matrix plagioclase (X_{An} = 0.30–0.32) and biotite (Fe/(Fe+Mg) = 0.45–0.47) are fairly uniform in composition. Rim compositions yield approximate P-T conditions of 3 kbar and 545°C, in good agreement with calculated phase relationships and garnet compositions.

An average age of 1890 ± 7 Ma (MSWD = 0.9) derives from eight SHRIMP analyses of three monazite grains (#11, 13, 196). Two of these occur in a domain with a gently folded S_1 fabric defined by biotite laths within a large andalusite porphyroblast (Fig. 9c). The third, monazite #196, is a well sealed inclusion that is aligned with ilmenite and a biotite inclusion within a garnet porphyroblast that does not have a clear relationship with foliation (Fig. 9c). An average age of 1805 ± 6 Ma (MSWD = 1.2) stems from 16 analyses of mostly equant, texturally late matrix grains (#35, 38, 183) that have some straight grain boundaries and irregular edges filling interstices or partially enclosing adjacent minerals, as well as monazite intersected by fractures within garnet (#252, 283), andalusite (#34), or in the matrix (#36, 214, 285). Monazite #197 and #194 are interpreted to have yielded mixed ages (ca. 1867, 1843 Ma, respectively), consistent with the location of these analyses across visible zones spatially related to fractures. Ages between 1780 and 1769 Ma correspond to brighter (BSE imaging) matrix grain rims (#38.1, 214.2), a more fractured garnet inclusion (#253), and a repeat analysis of a small matrix grain (#35). Monazite #195 occupies a fracture within garnet and is ca. 1730 Ma in age.

10SRB-G14 (GSC lab number 10591)

The most northerly sample analyzed was collected at the head of Padle Fiord (Fig. 2) from a resistant ridge exposing an imbricate panel of Hoare Bay cover rocks including ~15 m thick marble with lesser semipelite and minor interbedded psammite. Very strongly foliated semipelite in contact with marble was sampled from the limb of an outcrop-scale recumbent, gently north-plunging F_2 fold with a shallow northwest-dipping axial plane. The composite (S_0+S_1+S_2) foliation defined by biotite+sillimanite is oriented 275/33 with a strong extension lineation (L_2) plunging shallowly (8°) to the northwest (290°) parallel to the fold axis. Anhedral and variably embayed garnet porphyroblasts are pre-tectonic with respect to the main foliation (Fig. 10a). No P-T data were collected.

Thirty-two analyses of fourteen monazite grains range almost continuously from 1872 to 1834 Ma (Table 2). The thirteen oldest ages from eight monazite grains yield a mean age of 1861 ± 4 Ma (MSWD = 1.5, Fig. 10b), and correspond to darker (BSE imaging) zones furthest removed from fractures and brighter (BSE) rims. Six of these grains are oriented parallel to the main foliation of the rock (Fig. 10a), and one elongate monazite inclusion in garnet (#71) appears to overgrow S_2-aligned sillimanite inclusions (Fig. 10a upper inset). In contrast, twelve analyses (italicized in Table 2) of brighter BSE zones adjacent to rims and fractures of six grains yield a mean age of 1840 ± 3 Ma (MSWD = 0.97). A thin, fractured matrix grain (#34) gave a distinctly younger

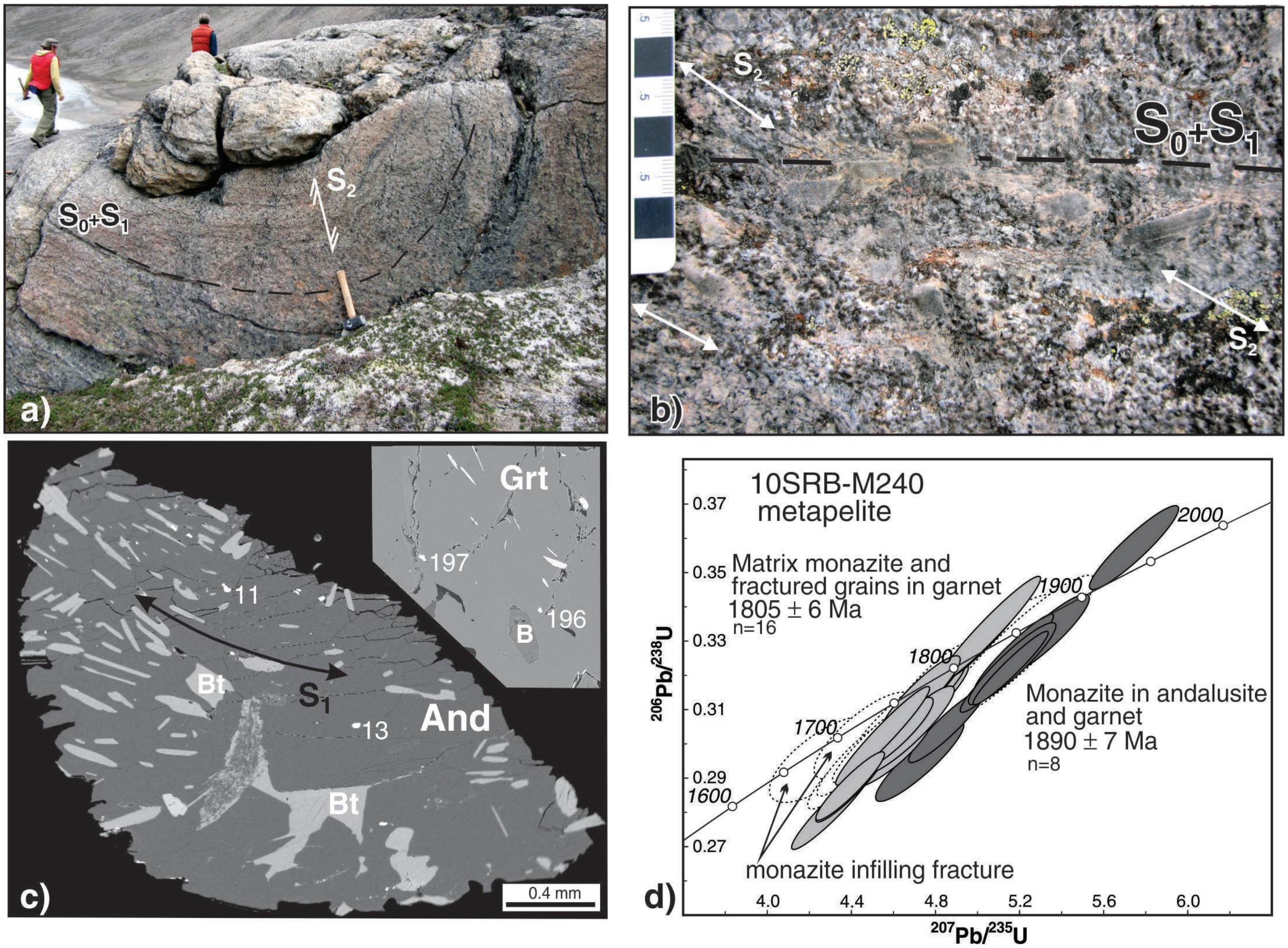

Figure 9. Sample M240, north shore of Totnes Road, Exeter Sound. **a)** Andalusite-porphyroblastic metapelite with bedding (S_0) parallel to S_1 cleavage, both folded into upright F_2 with weak axial planar S_2 at a high angle to S_0-S_1 in the hinge and at low angle to S_0-S_1 in the limbs. 2013-024. **b)** limb of F_2 fold at sample collection locality showing low angle between S_0-S_1 defined by andalusite porphyroblasts and axial planar S_2 defined by aligned biotite and elongate quartz. 2013-030. **c)** BSE image of andalusite (And) porphyroblast with biotite (Bt) defining the internal foliation. Upper inset shows a portion of garnet with aligned inclusions of ilmenite, monazite (numbered), and biotite. **d)** Concordia diagram of SHRIMP U-Pb results. Confidence ellipses and weighted mean $^{207}Pb/^{206}Pb$ ages are presented at the 95% confidence interval. Monazites from an older population present as inclusions in andalusite and garnet are shown in dark grey. Monazite found primarily in the matrix or within fractured garnets form a younger population shown in light grey. A subset of analyses from a number of textural settings interpreted to reflect mixed ages and excluded from the calculation of weighted mean ages are drawn as white ellipses with a dashed outline. *See* text for details.

age (1811 Ma). Seven intermediate ages (grey labels in Table 2), not included in either of these averaged groups, correspond to analyses that appear to have incorporated parts of both chemical zones.

DISCUSSION

The quantitative metamorphic and geochronological data presented above provide first-order constraints on the tectonometamorphic evolution of Cumberland Peninsula, with evidence for two Archean (M_{A1}, M_{A2}) and four Paleoproterozoic (M_{P1} to M_{P4}) episodes of monazite growth which constrain the timing of three deformational events (D_{A1}, D_{P1}, D_{P2}). The preliminary interpretations of these data given below will be further tested and elucidated through detailed textural and chemical studies as part of B. Hamilton's Ph.D. research.

Archean events (M_{A1} – D_{A1} and M_{A2})

Sample M32 records two Neoarchean episodes of monazite growth at 2785 ± 4 and 2701 ± 6 Ma. That ca. 2785 Ma monazite occurs as inclusions within the internal fabric of a garnet porphyroblast (Fig. 3a) suggests monazite growth

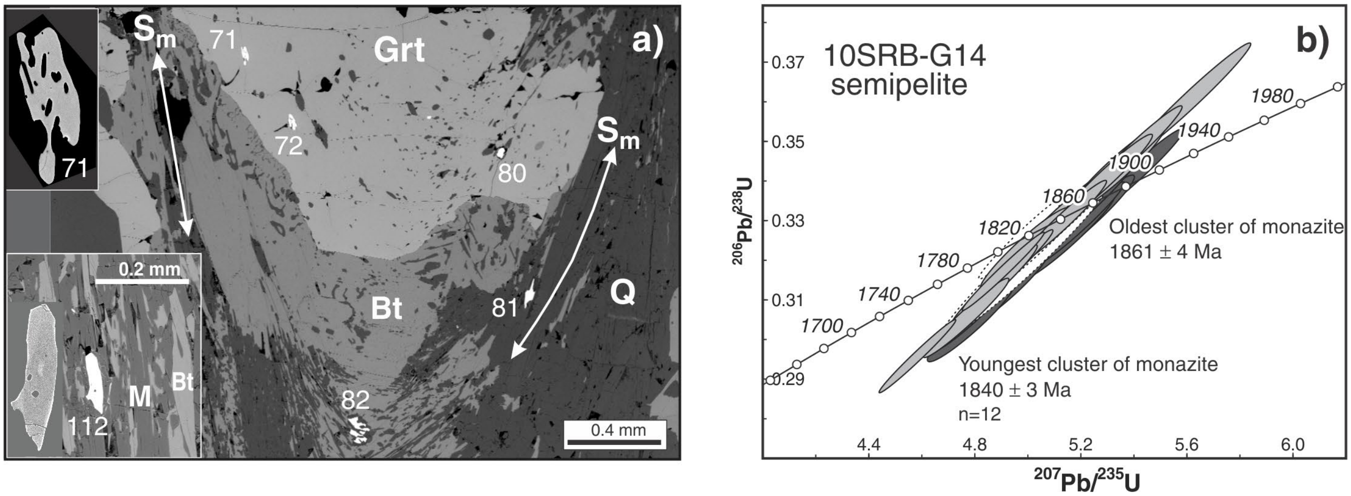

Figure 10. a) BSE image of textural relationships in G14. Note that sillimanite inclusions in monazite #71 (upper inset) are aligned with the S_2 foliation that is folded about the garnet porphyroblast that hosts three monazite grains (#71, 72, 80). Lower inset shows elongate monazite grain (#112) that is aligned with the foliation defined by muscovite (M) and biotite (Bt) in a different part of this rock. Note subtle BSE zonation in the enlarged image. **b)** Concordia diagram of SHRIMP U-Pb results. Confidence ellipses and weighted mean $^{207}Pb/^{206}Pb$ ages are presented at the 95% confidence interval. An older subset of monazite results is shown in dark grey, while a younger subset is shown in light grey. Analyses interpreted to reflect mixed ages and excluded from the calculation of weighted mean ages are drawn as white ellipses with a dashed outline. See text for details.

during an Archean deformation event (D_{A1}). Both ages are synchronous with regional plutonic events with tonalitic to granodioritic rocks of the peninsula dated at 2778 ± 5 Ma, 2760 ± 4 Ma, 2702 ± 5 Ma and 2695 ± 5 Ma (Rayner et al., 2012).

M_{P1}-D_{P1} at 1.90 – 1.88 Ga

Three samples contain monazite that crystallized between 1897 ± 8 and 1881 ± 8 Ma. These ages do not form a single statistical population (MSWD = 5.2), but they overlap with the timing of emplacement of the Qikiqtarjuaq plutonic suite, which has been dated between 1894 ± 6 and 1880 ± 5 Ma (Rayner et al., 2012). This supports the interpretation that monazite grew during regional contact metamorphism, which extended beyond the granulite-facies domains proximal to these intrusions (cf. Hamilton et al., 2012). Furthermore, the change from the absence of a fabric associated with the nominally oldest monazite inclusion in sample P30 to slightly to moderately elongate S_1-parallel younger monazite in samples H108 and M240 suggests that deformation progressed during pluton intrusion. This is consistent with occurrence of foliated metasedimentary xenoliths in a 1880 ± 5 Ma Qikiqtarjuaq pluton (Sanborn-Barrie et al., unpub. data).

M_{P2}-D_{P2} at 1.86 Ga

Six samples distributed across Cumberland Peninsula record monazite crystallization between 1863 ± 5 and 1859 ± 7 Ma (Table 1). That most of these ages derive from elongate, S_2-aligned monazite grains (Table 2) that in several instances host S_2-aligned sillimanite inclusions supports the conclusion that they effectively date the D_2 deformation event at amphibolite facies. The equant monazite in sample H90 may indicate weaker ca. 1860 Ma deformation at this location. The ca. 1860 Ma age of penetrative D_2 deformation is consistent with the brackets provided by the 1895 to 1880 Ma Qikiqtarjuaq plutonic suite that carries S_2 and a relatively weakly deformed 1836 ± 2 Ma leucogranite sill (N. Rayner unpub. data, 2011).

Amphibolite-facies deformation at ca. 1860 Ma has been identified at several locations in the Rae Craton (Fig. 1), including the northern domain of the Committee Bay belt (Berman et al., 2010a), Southampton Island (Berman et al., in press), and Melville Peninsula (Berman et al., unpub. data). As concluded in these other studies, this tectonometamorphic event is consistent with collision of Meta Incognita microcontinent with Cumberland Peninsula (presumed Rae Craton), which is constrained on western Baffin Island to have occurred between 1880 and 1865 Ma (St-Onge et al., 2006). If this collision occurred at ca. 1870 Ma, as suggested by thermal modelling of variably radiogenic crustal domains in the Committee Bay belt (Berman et al., 2010b), the short time lag (10 Ma) between collision, tectonic thickening, and monazite growth would be consistent with heating of the crust via magmatic advection (e.g. Qikiqtarjuaq plutonic suite) prior to and during tectonic thickening. Magmatism prior to inferred collision highlights the Qikiqtarjuaq suite as a potential pre-collisional continental arc, but geochemical analysis is required to assess this hypothesis. Further support for this tectonic setting derives from the dominant southerly vergence of ca. 1860 Ma D_2 structures on Cumberland

Peninsula which contrast with the north-vergent structures on central Baffin Island (St-Onge et al., 2006). This regional geometry resembles doubly vergent orogens observed in the upper plate of convergent margin settings (e.g. McDonough et al., 2000; Mueller et al., 2002).

M_{P3} at 1.84 Ga

Three samples from central Cumberland Peninsula yield results indicating monazite growth and/or recrystallization at ca. 1840 Ma (Table 1). Similar age, but non-reproducible analyses in three other samples (H108, H090, C49) cannot be interpreted with confidence because of the possibility that they represent mixed ages. In sample M82, ca. 1840 Ma monazite #49 is oriented perpendicular to the foliation, in association with a staurolite porphyroblast that cuts the foliation (Fig. 8c). These relationships suggest that D_2 deformation had waned by this time, but that significant decompression and cooling (to P-T conditions below staurolite stability; Hamilton et al., 2012) had not yet occurred. The absence of retrograde minerals in sample G14 (other than minor kaolinite adjacent to some plagioclase) also indicates that significant retrograde metamorphism had not occurred by this time, although the moderate relative yttrium content of a ca. 1840 Ma rim of monazite #181 in sample M32 suggests some garnet breakdown. Given these relationships, we interpret M_{P3} to likely represent a thermal peak to post-peak pulse of monazite growth ± recrystallization, possibly associated with garnet resorption during melt crystallization in the anatectic samples.

M_{P4} at 1.81 Ga

Monazite in sample M240 records a discrete population of younger ages (1805 ± 6 Ma) compared to other samples. M_{P4} monazite is interpreted to have crystallized at amphibolite-facies conditions not significantly below the thermal peak, based on the occurrence of sillimanite inclusions in monazite #183, along with the absence of retrograde minerals in this sample other than very minor biotite replacement by chlorite. In two other samples, single analyses of 1818 ± 8 Ma (sample C49) and 1813 ± 8 Ma (sample H108) may suggest more widespread monazite growth and/or recrystallization at this time. However, as only a limited number of matrix monazite grains were analyzed in most samples, further work is required to determine both the extent of, and metamorphic conditions associated with similar-aged matrix monazite on Cumberland Peninsula.

Conclusions

Preliminary in situ SHRIMP monazite geochronology reveals a polycyclic tectonometamorphic history for Cumberland Peninsula that contributes to regional tectonic and metallogenic models. In addition to two Neoarchean monazite growth events at 2785 ± 4 (M_{A1}-D_{A1}) and 2701 ± 6 Ma (M_{A2}), the data highlight at least four Paleoproterozoic events. Monazite ages between 1897 ± 8 and 1881 ± 8 Ma are interpreted to reflect regional contact metamorphism (M_{P1}) related to emplacement of the Qikiqtarjuaq plutonic suite, with textural features suggesting that D_{P1} deformation progressed during pluton intrusion. Monazite crystallization between 1863 ± 5 and 1859 ± 7 Ma is interpreted to date the main tectonometamorphic event (M_{P2}-D_{P2}) on Cumberland Peninsula, considered to reflect collision of Meta Incognita microcontinent with the Rae Craton. Monazite growth and/or recrystallization at ca. 1840 Ma (M_{P3}) and 1805 ± 6 Ma (M_{P4}) appears to have occurred after the thermal peak, during late- to post-tectonic, amphibolite-facies metamorphism.

ACKNOWLEDGMENTS

This project is part of the Geo-mapping for Energy and Minerals (GEM) initiative, with logistical field support in 2009 and 2010 provided by Natural Resources of Canada's Polar Continental Shelf Program (PCSP002–09, PCSP014–10). Mapping and sampling for this study were ably assisted by Carl Nagy, Greg Dobbelsteyn, and Matt Pointing. We thank Pat Hunt, Tom Pestaj, and Katherine Venance for assistance with acquiring SEM, SHRIMP, and microprobe data, respectively. Funding was provided by Natural Sciences and Engineering Research Council of Canada Discovery Grant 037233 to D. Pattison, and an Alexander Graham Bell Canada Graduate Scholarship and the W. Garfield Weston Award for Northern Research (Doctoral) to B. Hamilton. A constructive review was kindly provided by Dawn Kellett.

REFERENCES

Berman, R.G., 1991. Thermobarometry using multiequilibrium calculations: a new technique with petrological applications; Canadian Mineralogist, v. 29, p. 833–856.

Berman, R.G., 2007, winTWQ (version 2.3): A software package for performing internally-consistent thermobarometric calculations; Geological Survey of Canada Open File 5462, 41 p.doi:10.4095/223425

Berman, R.G., Sanborn-Barrie, M., Stern, R., and Carson, C., 2005. Tectonometamorphism at ca. 2.35 and 1.85 Ga in the Rae domain, western Churchill Province, Nunavut, Canada: insights from structural, metamorphic and in situ geochronological analysis of the southwestern Committee Bay belt; Canadian Mineralogist, v. 43, p. 409–442. doi:10.2113/gscanmin.43.1.409

Berman, R.G., Sanborn-Barrie, M., Rayner, N., Carson, C., Sandeman, H., and Skulski, T., 2010a. Petrological and in situ SHRIMP geochronological constraints on tectonometamorphic evolution of the Committee Bay belt, Nunavut; Precambrian Research, v. 181, p. 1–20. doi:10.1016/j.precamres.2010.05.009

Berman, R.G., Sandeman, H.A.I., and Camacho, A., 2010b. Diachronous deformation and metamorphism in the Committee Bay belt, Rae Province, Nunavut: insights from ^{40}Ar-^{39}Ar cooling ages and thermal modelling; Journal of Metamorphic Geology, v. 28, p. 439–457. doi:10.1111/j.1525-1314.2010.00873.x

Berman, R.G., Rayner, N., Sanborn-Barrie, M., and Whalen, J., in press: The tectonometamorphic evolution of Southampton Island, Nunavut: insight from petrologic modeling and in situ SHRIMP geochronology of multiple episodes of monazite growth; Precambrian Research. doi:10.1016/j.precamres.2012.08.011

Corrigan, D., Perhsson, S., Wodicka, N., and de Kemp, E., 2009. The Palaeoproterozoic Trans-Hudson Orogen: a prototype of modern accretionary processes; Geological Society London Special Publication, v. 327, p. 457–479. doi:10.1144/SP327.19

de Capitani, C. and Petrakakis, K., 2010. The computation of equilibrium assemblage diagrams with Theriak/Domino software; The American Mineralogist, v. 95, p. 1006–1016. doi:10.2138/am.2010.3354

Hamilton, B., Pattison, D.M., Sanborn-Barrie, M., and Young, M., 2012: Preliminary characterization of metamorphism on Cumberland Peninsula, Baffin Island, Nunavut; Geological Survey of Canada, Current Research 2012-9, 20 p. doi:10.4095/291530

Jackson, G.D., 1971. Operation Penny Highlands, south-central Baffin Island; Geological Survey of Canada, Paper, v. 71–1A, p. 138–140.

Keim, R., Sanborn-Barrie, M., Ansdell, K., and Young, M., 2011. Totnes Road metavolcanic rocks: a fragmental, Ti-enriched komatiitic volcanic suite on Cumberland Peninsula, Baffin Island, Nunavut; Geological Survey of Canada, Current Research 2011-13. 18 p. doi:10.4095/289072

McDonough, M.R., McNicoll, V.J., Schetselaar, E.M., and Grover, W., 2000. Geochronological and kinematic constraints on crustal shortening and escape in a two-sided oblique-slip collisional and magmatic orogen, Paleoproterozoic Taltson magmatic zone, northeastern Alberta; Canadian Journal of Earth Sciences, v. 37, p. 1549–1573. doi:10.1139/e00-089

Mueller, J., Kley, J., and Jacobshagen, V., 2002, Structure and Cenozoic kinematics of the Eastern Cordillera, southern Bolivia (21 °S), Tectonics, v. 21, p. doi:10.1029/2001tc001340

Rayner, N. and Stern, R.A., 2002. Improved sample preparation method for SHRIMP analysis of delicate mineral grains exposed in thin sections; Geological Survey of Canada, Current Research 2002-F10, 3 p. doi:10.4095/213203

Rayner, N., Sanborn-Barrie, M., Young, M., and Whalen, J.B., 2012. U-Pb ages of Archean basement and Paleoproterozoic plutonic rocks, southern Cumberland Peninsula, eastern Baffin Island, Nunavut; Geological Survey of Canada, Current Research 2012-8, p. 28 p. doi:10.4095/291401

Sanborn-Barrie, M. and Young, M., 2013a. Geology, Circle Lake, Nunavut; Geological Survey of Canada, Canadian Geoscience Map 5, (preliminary edition), scale 1:100 000. doi:10.4095/288929

Sanborn-Barrie, M. and Young, M., 2013b. Geology, Padle Fiord, Nunavut; Geological Survey of Canada, Canadian Geoscience Map 37, (preliminary edition), scale 1:100 000. doi:10.4095/292014

Sanborn-Barrie, M. and Young, M., 2013c. Geology, Durban Harbour, Nunavut; Geological Survey of Canada, Canadian Geoscience Map 38, (preliminary edition), scale 1:100 000. doi:10.4095/292015

Sanborn-Barrie, M., Young, M., Whalen, J., and James, D., 2011a. Geology, Ujuktuk Fiord, Nunavut; Geological Survey of Canada, Canadian Geoscience Map 1, (2nd edition, preliminary), scale 1:100 000. doi:10.4095/289237

Sanborn-Barrie, M. and Young, M., and Whalen, J., 2011b. Geology, Kingnait Fiord, Nunavut; Geological Survey of Canada, Canadian Geoscience Map 2, (2nd edition, preliminary), scale 1:100 000. doi:10.4095/289238

Sanborn-Barrie, M., Young, M., Whalen, J., James, D., and St-Onge, M.R., 2011c. Geology, Touak Fiord, Nunavut; Geological Survey of Canada, Canadian Geoscience Map 3, (2nd edition, preliminary), scale 1:100 000. doi:10.4095/289239

Sanborn-Barrie, M., Young, M., Keim, R., and Hamilton, B.M., 2013a. Geology, Sunneshine Fiord, Nunavut; Geological Survey of Canada, Canadian Geoscience Map 6, (preliminary edition), scale 1:100 000. doi:10.4095/288931

Sanborn-Barrie, M., Young, M., and Whalen, J., 2013b. Geology, Qikiqtarjuaq, Nunavut; Geological Survey of Canada, Canadian Geoscience Map 39, (preliminary edition), scale 1:100 000. doi:10.4095/292016

St-Onge, M.R., Searle, M.P., and Wodicka, N., 2006. Trans-Hudson Orogen of North America and Himalaya-Karakoram-Tibetan Orogen of Asia; structural and thermal characteristics of the lower and upper plates; Tectonics, v. 25, cit. no. TC4006. doi:10.1029/2005TC001907

St-Onge, M.R., van Gool, J., Garde, A., and Scott, D.J., 2009. Correlation of Archaean and Palaeoproterozoic units between northeastern Canada and western Greenland: constraining the pre-collisional upper plate accretionary history of the Trans-Hudson orogen; *in* Earth Accretionary Systems in Space and Time, (ed.) P.A.K. Cawood; Geological Society of London, Special Publication, v. 318, p. 193–235.

Stern, R.A., 1997. The GSC Sensitive High Resolution Ion Microprobe (SHRIMP): analytical techniques of zircon U-Th-Pb age determinations and performance evaluation; *in* Current Research 1997-F; Geological Survey of Canada, p. 1–31.

Stern, R.A. and Berman, R.G., 2001. Monazite U-Pb and Th-Pb geochronology by ion microprobe, with an application to in situ dating of an Archean metasedimentary rock; Chemical Geology, v. 172, p. 113–130. doi:10.1016/S0009-2541(00)00239-4

Geological Survey of Canada Project MGM007